Open Journal of Modelling and Simulation, 2026, 14(4), 147-195
https://www.scirp.org/journal/ojmsi
ISSN Online: 2327-4026
ISSN Print: 2327-4018

The Exterior Green Function of the Mandelbrot Set: Conformal Construction and Quantitative Escape-Rate Approximation

Abhirup Moitra

Department of Mathematics, University of Essex, Colchester, United Kingdom
Email: am25763@essex.ac.uk

How to cite this paper: Moitra, A. (2026) The Exterior Green Function of the Mandelbrot Set: Conformal Construction and Quantitative Escape-Rate Approximation. *Open Journal of Modelling and Simulation*, **14**, 147-195.
https://doi.org/10.4236/ojmsi.2026.144008

Received: July 21, 2026
Accepted: September 20, 2026
Published: September 23, 2026

Abstract

For the quadratic family $f_c(z) = z^2 + c$, we study the exterior Green function of the Mandelbrot set $\mathcal{M}$ through classical conformal uniformization, logarithmic potential theory, and quantitative escape-rate approximation. As classical input, we use the Douady–Hubbard parameter Böttcher map $\Phi_{\mathcal{M}} : \mathbb{C} \setminus \mathcal{M} \to \mathbb{C} \setminus \overline{\mathbb{D}}$, normalized at infinity, and the representation $G_{\mathcal{M}}(c) = \log\left|\Phi_{\mathcal{M}}(c)\right|$. The harmonicity and positivity of $G_{\mathcal{M}}$ on $\mathbb{C} \setminus \mathcal{M}$, its continuous extension by zero on $\mathcal{M}$, its normalized logarithmic growth at infinity, its uniqueness as the normalized exterior Green function, and the identity $G_{\mathcal{M}}(c) = g_c(c) = 2g_c(0)$ are classical facts recalled to fix the analytic framework and normalization. The quantitative escape-rate estimate used in this paper was established in the author's earlier work. The contribution of the present paper is to provide a self-contained telescoping derivation and to identify the parameter-plane conformal meaning of that estimate through the preceding classical identity. Through this interpretation, the previously established $O\left(2^{-n}\right)$ escape-rate estimate becomes an explicit quantitative approximation of the parameter Böttcher potential by the normalized finite critical orbit approximants. We further obtain uniform exponential convergence on compact subsets of $\mathbb{C} \setminus \mathcal{M}$, prove Hausdorff continuity of positive equipotentials over compact level ranges, and formulate fixed-index and variable-time numerical procedures consistent with the analytic normalization. For detected escaping parameters, the variable-time first-escape estimator is accompanied by an explicit pointwise error certificate. The numerical figures are finite-resolution illustrations of the analytic results and do not certify membership in $\mathcal{M}$ on the unresolved finite-time mask.

Keywords

Mandelbrot Set, Green Function, Böttcher Coordinate, Exterior Uniformization, Escape-Rate Approximation, Equipotentials

1. Introduction

The quadratic family $f_c(z)=z^2+c, c\in\mathbb{C}$ introduced formally in Definition 3.1, occupies a central position in one-dimensional holomorphic dynamics. For a fixed parameter c, its dynamical-plane structure is encoded by the filled Julia set K_c, the Julia set $J_c=\partial K_c$, and the basin of infinity $A_c(\infty)=\mathbb{C}\setminus K_c$. Its parameter-space organization is governed by the Mandelbrot set

$$\mathcal{M}=\left\{c\in\mathbb{C}:\left\{f_c^{\circ n}(0)\right\}_{n\geq 0}\text{ is bounded}\right\}. \tag{1}$$

The formal definition is given in Definition 3.3. The critical orbit $0, f_c(0)=c, f_c^{\circ 2}(0),\cdots$ therefore determines whether the parameter belongs to $\mathcal{M}$ or to its complement.

In the classical theory developed by Douady and Hubbard, the exterior $\mathbb{C}\setminus\mathcal{M}$ admits a normalized conformal uniformization

$$\Phi_{\mathcal{M}}:\mathbb{C}\setminus\mathcal{M}\to\mathbb{C}\setminus\overline{\mathbb{D}},\quad \frac{\Phi_{\mathcal{M}}(c)}{c}\to 1\ (c\to\infty). \tag{2}$$

Under the uniformization (2), the associated parameter Green function is represented by

$$G_{\mathcal{M}}(c)=\log\left|\Phi_{\mathcal{M}}(c)\right|. \tag{3}$$

The representation (3), together with the classical properties of $\Phi_{\mathcal{M}}$, yields the harmonicity and strict positivity of $G_{\mathcal{M}}$ on $\mathbb{C}\setminus\mathcal{M}$, its continuous extension by zero on $\mathcal{M}$, and its normalized logarithmic growth

$$G_{\mathcal{M}}(c)-\log|c|\to 0\ (c\to\infty). \tag{4}$$

The boundary condition and the growth condition (4) enter the classical uniqueness characterization of $G_{\mathcal{M}}$ as the normalized exterior Green function with pole at infinity. The same conformal coordinate determines the classical parameter equipotentials and external rays. These facts are standard consequences of classical exterior uniformization and logarithmic potential theory. They are recalled here to establish the analytic framework and normalization required for the subsequent quantitative analysis; see [1]-[5]. The relationship between the dynamical-plane and parameter-plane normalizations is likewise classical. Let g_c denote the dynamical Green function of f_c. Its functional equation is

$$g_c\left(f_c(z)\right)=2g_c(z). \tag{5}$$

Applying (5) at $z=0$, together with $f_c(0)=c$, gives

$$G_{\mathcal{M}}(c)=g_c(c)=2g_c(0),\ c\in\mathbb{C}\setminus\mathcal{M}. \tag{6}$$

Combining (3) and (6) gives the complete normalization identity

$$G_{\mathcal{M}}(c) = \log\left|\Phi_{\mathcal{M}}(c)\right| = g_c(c) = 2g_c(0). \tag{7}$$

The classical identity (7) provides the bridge between critical orbit escape and the parameter Böttcher potential. The representation of $G_{\mathcal{M}}$ by the parameter Böttcher map, its standard potential-theoretic properties, its uniqueness characterization, and the preceding dynamical–parameter identity are not claimed as new results. They are included to provide a self-contained structural setting and to establish the precise normalization used throughout the paper.

For the critical orbit

$$z_0(c) = 0,\ \ z_{n+1}(c) = z_n(c)^2 + c. \tag{8}$$

consider the finite escape-rate approximants

$$G_n(c) = \frac{1}{2^n}\log^+\left|z_n(c)\right| = \frac{1}{2^n}\log^+\left|f_c^{\circ n}(0)\right|. \tag{9}$$

The quantitative escape-rate estimate governing the approximants in (9) was established in the author's earlier work [6]. Accordingly, the estimate considered in isolation is not claimed as a new result of the present paper.

For completeness, the present manuscript gives a self-contained telescoping derivation directly from the critical orbit recurrence in (8). More importantly, the present manuscript identifies the parameter-plane conformal meaning of the estimate through the classical normalization identity (7). Through the identification (7), the normalized finite critical orbit quantities

$$A_n(c) := 2G_n(c). \tag{10}$$

become quantitative approximations to the parameter Böttcher potential. Once the critical orbit has entered a prescribed escape region, Theorem 8.1 gives an explicit estimate of the form

$$\left|2G_n(c) - \log\left|\Phi_{\mathcal{M}}(c)\right|\right| \le C(c,R)2^{-n}. \tag{11}$$

In (11), the constant $C(c,R)$ is independent of n. Thus, through the conformal interpretation developed here, the previously established escape-rate estimate becomes an explicit approximation result for the exterior Green function of the Mandelbrot set. The pointwise estimate (11) admits a uniform compact-subset consequence. The present paper also obtains uniform exponential convergence on every compact subset of $\mathbb{C}\setminus\mathcal{M}$. More precisely, if $K \subset \mathbb{C}\setminus\mathcal{M}$ is compact, then Corollary 8.4 provides common constants $n_K \ge 1$ and $C_K > 0$ such that

$$\sup_{c\in K}\left|2G_n(c) - G_{\mathcal{M}}(c)\right| \le C_K 2^{-n},\ \ n \ge n_K. \tag{12}$$

The compact-uniform estimate (12) clarifies why a common finite iteration depth can approximate $G_{\mathcal{M}}$ reliably on parameter regions lying a positive distance from $\partial\mathcal{M}$. It also identifies the boundary as the region in which no global common escape time should be expected.

The numerical methodology is formulated to preserve the distinction between fixed-index approximation and parameter-dependent escape detection. For a prescribed index N, the fixed-index field is

$$A_N(c) = 2G_N(c). \tag{13}$$

This quantity uses the same iteration index for every parameter. By contrast, the variable-time first-escape estimator is

$$\hat{G}_{\text{esc}}(c) = 2G_{\tau_{N_{\max}}(c)}(c). \tag{14}$$

where $\tau_{N_{\max}}(c)$ is the first index, not exceeding the iteration budget $N_{\max}$, at which the critical orbit crosses the chosen escape radius. The estimators in (13) and (14) coincide only when $N = \tau_{N_{\max}}(c)$. They are therefore kept notationally and computationally distinct. For every parameter whose escape is detected, the first-escape estimator is accompanied by the explicit pointwise certificate

$$\left|\hat{G}_{\text{esc}}(c) - G_{\mathcal{M}}(c)\right| \le \hat{E}_{\text{esc}}(c). \tag{15}$$

The certificate (15) applies only when escape is detected and the stated admissibility condition on the escape radius is satisfied. If escape is not detected within the prescribed iteration budget, the parameter is placed in a finite-time unresolved mask. This numerical outcome records only the failure to detect escape and does not certify membership in $\mathcal{M}$. The corresponding dark regions in the figures must therefore not be interpreted as rigorous numerical representations of the Mandelbrot set.

The convergence visualization similarly distinguishes the exact Green function from a certified numerical reference. If $G_{\text{ref}}(c)$ is a first-escape reference computed using a large reference radius and

$$\left|G_{\text{ref}}(c) - G_{\mathcal{M}}(c)\right| \le E_{\text{ref}}(c). \tag{16}$$

then the triangle inequality gives

$$\left|A_n(c) - G_{\text{ref}}(c)\right| \le B_n(c;R) + E_{\text{ref}}(c). \tag{17}$$

Here $B_n(c;R)$ is the bound supplied by Theorem 8.1. The right-hand side of (17) is the certified comparison bound represented by the dotted curves in the convergence **Figure 5**.

The exterior conformal representation also gives the identity for every positive equipotential

$$\begin{aligned} E_t &:= \left\{c \in \mathbb{C} \setminus \mathcal{M} : G_{\mathcal{M}}(c) = t\right\} \\ &= \Phi_{\mathcal{M}}^{-1}(C_t), \text{ where, } C_t := \left\{w \in \mathbb{C} : |w| = \mathrm{e}^t\right\}. \end{aligned} \tag{18}$$

The present paper proves that the family of equipotentials varies continuously in the Hausdorff metric over every compact positive level range. More precisely, Theorem 9.1 shows that if $0 < a < b$, $t_n, t \in [a,b]$, and $t_n \to t$, then

$$d_{\mathrm{H}}\left(E_{t_n}, E_t\right) \to 0. \tag{19}$$

The convergence in (19) concerns the exact equipotentials of $G_{\mathcal{M}}$. The numerical level curves displayed later are finite-resolution illustrations of the theorem and are not used in its proof.

The computed exterior-geometry figure also uses a truncated approximation to the Böttcher logarithm in order to visualize numerical external-angle fields and parameter-ray segments. These objects are included only as finite-resolution approximations. No global branch-certified error estimate for $\arg\Phi_{\mathcal{M}}$ is claimed, and the extracted numerical ray components are not identified with exact external rays.

The contributions developed in the present paper may therefore be summarized as follows:

(i) A self-contained telescoping derivation of the previously established quantitative escape-rate estimate;

(ii) An explicit interpretation of that estimate as an approximation to the parameter Böttcher potential $\log\left|\Phi_{\mathcal{M}}(c)\right|$;

(iii) Uniform exponential convergence of the normalized finite critical orbit approximants on compact subsets of $\mathbb{C}\setminus\mathcal{M}$;

(iv) A precise distinction between fixed-index approximation and variable-time first-escape estimation, including a pointwise error certificate for detected escaping parameters;

(v) A certified comparison bound for the discrepancy between fixed-index approximants and the numerical first-escape reference;

(vi) Hausdorff continuity of the exact equipotentials over compact positive level ranges;

(vii) Finite-resolution numerical procedures whose notation and normalization are consistent with the analytic quantities being approximated.

The emphasis of the present article therefore differs from that of the author's earlier work [6]. The earlier paper developed the effective quantitative behaviour of regularized critical orbit escape. The present paper places that estimate within the classical exterior conformal geometry of the Mandelbrot set, supplies the telescoping derivation for self-containment, derives the compact-uniform consequence, formulates the certified first-escape comparison, and establishes the positive-level equipotential-stability result. Accordingly, the contributions of the present article lie in the quantitative–conformal interpretation, its compact-uniform consequence, the certified formulation of the numerical approximations, and the Hausdorff stability analysis. The classical construction of the parameter Green function, its standard potential-theoretic properties, its uniqueness characterization, the dynamical–parameter normalization, and the escape-rate estimate considered independently are not claimed as new results.

The paper is organized as follows. Section 2 reviews the relevant literature and places the present work in its mathematical context. Section 3 introduces the definitions and normalizations used throughout the paper. Section 4 recalls the classical dynamical Böttcher coordinate, its holomorphic dependence near infinity, and the Douady–Hubbard parameter uniformization, summarized schematically in **Figure 1**. Section 5 records the classical exterior conformal representation of the parameter Green function and derives its standard potential-theoretic properties. Section 6 gives, for completeness, a direct maximum-principle proof of the classical uniqueness characterization. Section 7 recalls the exact conformal description of equipotentials and external rays. Section 8 gives the self-contained telescoping derivation, establishes the quantitative–conformal interpretation, derives uniform exponential convergence on compact exterior parameter sets, and introduces the numerical procedures used in **Figures 2-5**. Section 9 proves Hausdorff continuity of equipotentials over compact positive level ranges, illustrated in **Figure 6**. Section 10 explains the relation between the present conformal interpretation and the author's earlier quantitative study. Section 11 records the limitations of the present analysis, and Section 12 formulates the proposed directions for future research. The paper concludes in Section 13.

2. Literature Review and Mathematical Context

The modern study of quadratic complex dynamics is rooted in the work of Douady and Hubbard, who developed the foundational theory of polynomial-like mappings, external uniformization, and the parameter-space description of the Mandelbrot set [2] [3]. In their framework, the Mandelbrot set appears as the connectedness locus for the quadratic family, while its complement is naturally described by a Green function with pole at infinity. Earlier potential-theoretic foundations of polynomial iteration, including invariant sets and capacity, go back to Brolin's work [7].

A standard and geometrically transparent account of these ideas is given by Milnor [5], who emphasizes the role of critical orbits, Julia sets, Böttcher coordinates, and external rays in one-dimensional holomorphic dynamics. Closely related presentations appear in Carleson and Gamelin [1] and in Beardon's classical treatment of iteration theory [8]. For broader analytic and geometric background, including Teichmüller-theoretic aspects and the global organization of parameter space, one may also consult Hubbard [4].

From the standpoint of analysis, the Green function of $\mathbb{C} \setminus \mathcal{M}$ belongs to classical logarithmic potential theory. Its basic properties—harmonicity on the complement, vanishing on the compact set, and logarithmic growth at infinity—fit naturally into the theory of harmonic and subharmonic functions, planar Green functions, Dirichlet problems, and conformal mapping. Useful background for these topics may be found in Ransford [9] and in Axler, Bourdon, and Ramey [10]. In parameter spaces of rational maps, potential-theoretic and Green-function ideas also underlie bifurcation currents and Lyapunov-exponent methods, as developed for example by DeMarco [11] and Dujardin–Favre [12]. For Green functions in varying polynomial families, see also Favre–Gauthier [13].

Recent developments show that the geometry of the Mandelbrot set and of related parameter spaces continues to evolve in several active directions. These include renormalization and local-connectivity phenomena associated with the Mandelbrot set and the MLC programme [14], self-similarity near Siegel parameters and pacman renormalization [15], positive-area phenomena for quadratic

Julia sets [16], continuity and limiting behaviour for Julia sets and invariant external rays [17], richer parameter-space structures in cubic and parabolic settings [18], and Mandelbrot-type analogues in broader polynomial and transcendental families [19] [20]. In this broader context, the present paper remains within the classical quadratic setting, but its emphasis lies at the intersection of exterior conformal uniformization, logarithmic potential theory, and the structural interpretation of escape-rate regularization.

The present article should be read together with [6]. In that work, the principal object was the regularized critical orbit escape-rate function

$$\mathcal{G}(c) := \lim_{n\to\infty} \frac{1}{2^n} \log^+ \left| f_c^{\circ n}(0) \right|. \tag{20}$$

The function in (20) was studied as a quantitatively tractable observable of escape. The present article is a geometric companion: the earlier paper studies the effective quantitative behaviour of regularized escape, whereas the present paper identifies the structural analytic object underlying that theory and proves a bridge theorem between the two viewpoints.

3. Preliminaries and Normalizations

Definition 3.1 (Quadratic Family). For $c \in \mathbb{C}$, define

$$f_c : \mathbb{C} \to \mathbb{C}, \quad f_c(z) = z^2 + c. \tag{21}$$

Its n-fold iterate is denoted by $f_c^{\circ n}$.

Definition 3.2 (Filled Julia set, Julia set, and Basin of Infinity [1], Chapter VI and [5] Chapter 8). For fixed $c \in \mathbb{C}$, the filled Julia set of f_c is

$$K_c := \left\{ z \in \mathbb{C} : \sup_{n\ge 0} \left| f_c^{\circ n}(z) \right| < \infty \right\}. \tag{22}$$

the Julia set is

$$J_c := \partial K_c. \tag{23}$$

and the basin of infinity is

$$A_c(\infty) := \mathbb{C} \setminus K_c. \tag{24}$$

Definition 3.3 (Mandelbrot Set, [2] [3] and [5], Chapter 14). The Mandelbrot set is

$$\mathcal{M} := \left\{ c \in \mathbb{C} : \sup_{n\ge 0} \left| f_c^{\circ n}(0) \right| < \infty \right\}. \tag{25}$$

Equivalently, $c \in \mathcal{M}$ if and only if the critical orbit of f_c is bounded.

Definition 3.4 (Positive Logarithm). For $r \ge 0$, define

$$\log^+ r := \log \max\{r, 1\}. \tag{26}$$

For $r > 0$, the definition is equivalently written as

$$\log^+ r = \max\{\log r, 0\}. \tag{27}$$

Definition 3.5 (Dynamical Green Function) ([1] Chapter VI and [5] Chapter 8). For each $c \in \mathbb{C}$, the dynamical Green function of $f_c(z) = z^2 + c$ is

$$g_c(z) := \lim_{n\to\infty} \frac{1}{2^n} \log^+ \left| f_c^{\circ n}(z) \right|. \tag{28}$$

Here $\log^+$ is defined in (26). It is a classical theorem that the limit in (28) exists for every $z \in \mathbb{C}$.

Definition 3.6 (Finite Critical Orbit Escape Rate Approximants). For $c \in \mathbb{C}$, let

$$z_0 = 0, \; z_{n+1} = f_c(z_n) = z_n^2 + c. \tag{29}$$

For $n \geq 0$, define

$$G_n(c) := \frac{1}{2^n} \log^+ |z_n| = \frac{1}{2^n} \log^+ \left| f_c^{\circ n}(0) \right|. \tag{30}$$

The quantities defined in (30) are the finite critical orbit regularizations used later in Theorem 8.1 and in the numerical schemes of Section 8.1. The recurrence (29) is used in the telescoping argument of Theorem 8.1.

By the defining limit (28), evaluated at $z = 0$, and the definition in (30), one has

$$g_c(0) = \lim_{n\to\infty} G_n(c). \tag{31}$$

***Remark* 3.7 (Classical Properties of g_c).** It is classical that for every $c \in \mathbb{C}$, the function g_c defined in (28) exists on all of $\mathbb{C}$, vanishes precisely on K_c, is harmonic on $A_c(\infty)$, and satisfies the functional equation

$$g_c(f_c(z)) = 2g_c(z). \tag{32}$$

See [1], Chapter VI, or [5], Chapter 8.

Definition 3.8 (Logarithmic Pole at Infinity). Let $\Omega \subset \mathbb{C}$ be an unbounded domain whose complement is compact. A real-valued function u on Ω has a logarithmic pole at infinity with the normalization used in this paper if

$$u(c) - \log|c| \to 0 \; (c \to \infty). \tag{33}$$

Equivalently, $u(c) = \log|c| + o(1)$ as $c \to \infty$. This is the normalization used for the Green function of $\mathbb{C} \setminus \mathcal{M}$.

Definition 3.9 (Parameter Green Function, Dynamical Normalization). For $c \in \mathbb{C} \setminus \mathcal{M}$, define initially

$$G_{\mathcal{M}}(c) := g_c(c). \tag{34}$$

The dynamical normalization (34) will be identified in Proposition 5.3 with the exterior conformal formula introduced in Definition 5.1.

***Remark* 3.10 (Normalization Bridge).** The normalization in Definition 3.9 is naturally compatible with the parameter-plane Böttcher map introduced in Notation 3.11. It differs by a factor 2 from the critical-point normalization $\mathcal{G}(c) := g_c(0)$ used in [6]. Since $f_c(0) = c$, the functional Equation (32) gives

$$G_{\mathcal{M}}(c) = g_c(c) = g_c(f_c(0)) = 2g_c(0) = 2\mathcal{G}(c), \; c \in \mathbb{C} \setminus \mathcal{M}. \tag{35}$$

The identity (35) shows that the two normalizations encode the same escape geometry, but they are adapted to different viewpoints: $\mathcal{G}$ is suited to critical orbit regularization, whereas $G_{\mathcal{M}}$ is suited to parameter-plane exterior uniformization.

Notation 3.11 (Parameter Böttcher Map). Throughout the paper, $\Phi_{\mathcal{M}}$ denotes the conformal map $\Phi_{\mathcal{M}}:\mathbb{C}\setminus\mathcal{M}\to\mathbb{C}\setminus\overline{\mathbb{D}}$ normalized by

$$\frac{\Phi_{\mathcal{M}}(c)}{c}\to 1\ \left(c\to\infty\right). \tag{36}$$

This map is recalled more formally in Theorem 4.8.

Definition 3.12 (Hausdorff Distance). Let $A,B\subset\mathbb{C}$ be nonempty compact sets. Their Hausdorff distance is

$$d_{\mathrm{H}}\left(A,B\right):=\max\left\{\sup_{a\in A}\inf_{b\in B}\left|a-b\right|,\sup_{b\in B}\inf_{a\in A}\left|a-b\right|\right\}. \tag{37}$$

The metric (37) is used in Theorem 9.1 to measure stability of equipotentials.

Notation 3.13 (Exterior Circles and Compact Annuli). For $t>0$, write

$$C_t:=\left\{w\in\mathbb{C}:\left|w\right|=\mathrm{e}^t\right\}. \tag{38}$$

For $0<a<b$, write

$$A_{a,b}:=\left\{w\in\mathbb{C}:\mathrm{e}^a\le\left|w\right|\le\mathrm{e}^b\right\}. \tag{39}$$

***Remark* 3.14** (Compact Subsets of the Exterior). If $K\subset\mathbb{C}\setminus\mathcal{M}$ is a nonempty compact set, then K lies at a positive Euclidean distance from $\mathcal{M}$. Equivalently,

$$\operatorname{dist}\left(K,\mathcal{M}\right):=\inf\left\{\left|c-\zeta\right|:c\in K,\zeta\in\mathcal{M}\right\}>0. \tag{40}$$

This positive separation does not by itself provide a common escape time for all parameters in K. In the proof of Corollary 8.4, continuity of the critical orbit polynomials from Notation 4.4, together with a finite-subcover argument, is used to construct the common entry index n_K defined in (129).

4. Classical Exterior Uniformization and the Parameter Böttcher Map

We recall the classical Böttcher coordinate near infinity and the corresponding parameter-space uniformization. These results provide the conformal input used in Definition 5.1 and Proposition 5.3.

Theorem 4.1 (Böttcher Coordinate near Infinity) *Fix* $c\in\mathbb{C}$. *There exist a neighbourhood* U_c *of infinity, a number* $R_c>1$, *and a unique conformal map* $\phi_c:U_c\to\left\{w\in\mathbb{C}:\left|w\right|>R_c\right\}$ *such that*

$$\phi_c\left(f_c\left(z\right)\right)=\left(\phi_c\left(z\right)\right)^2. \tag{41}$$

whenever $z,f_c\left(z\right)\in U_c$, and $\dfrac{\phi_c\left(z\right)}{z}\to 1$ as $z\to\infty$. Moreover,

$$g_c\left(z\right)=\log\left|\phi_c\left(z\right)\right|\ \left(z\in U_c\right). \tag{42}$$

Proof. This is the classical Böttcher theorem applied to the super-attracting fixed point at infinity of $f_c(z)=z^2+c$; see [8], Chapter 3, [1], Chapter VI, and [5], Chapter 8. For z sufficiently large,

$$f_c(z)=z^2\left(1+\frac{c}{z^2}\right). \tag{43}$$

The factorization (43) shows that the correction term c/z^2 is small near infinity. The standard Böttcher iteration construction produces a holomorphic function ϕ_c, defined in an exterior neighbourhood of infinity, satisfying (41) and $\phi_c(z)=z+O(1)$ as ($z\to\infty$). The stronger normalization $\frac{\phi_c(z)}{z}\to 1$ determines ϕ_c uniquely.

For completeness, the construction can be written locally in the form

$$\phi_c(z)=z\exp\left(\sum_{j=0}^{\infty}\frac{1}{2^{j+1}}\operatorname{Log}\left(1+\frac{c}{\left(f_c^{\circ j}(z)\right)^2}\right)\right). \tag{44}$$

In the representation (44), the neighbourhood of infinity is chosen so that

$$\left|\frac{c}{\left(f_c^{\circ j}(z)\right)^2}\right|<1,\quad \forall j\ge 0. \tag{45}$$

Here, Log denotes the branch satisfying $\operatorname{Log}1=0$. Condition (45) ensures that the logarithmic terms are evaluated in a common neighbourhood of 1. The series in (44) converges locally uniformly near infinity and therefore defines a holomorphic function there. Finally, by the defining limit (28), the dynamical Green function is obtained from the normalized asymptotic growth of $f_c^{\circ n}(z)$. For $z\in U_c$, the orbit tends to infinity, and the Böttcher functional equation gives

$$\phi_c\left(f_c^{\circ n}(z)\right)=\left(\phi_c(z)\right)^{2^n}. \tag{46}$$

Taking absolute values and logarithms in (46) gives

$$\frac{1}{2^n}\log\left|\phi_c\left(f_c^{\circ n}(z)\right)\right|=\log\left|\phi_c(z)\right|. \tag{47}$$

Since $\frac{\phi_c(w)}{w}\to 1$ as ($w\to\infty$), the difference between $\log\left|\phi_c\left(f_c^{\circ n}(z)\right)\right|$ and $\log\left|f_c^{\circ n}(z)\right|$ tends to zero. Combining the defining limit (28) with (47) therefore proves the identity (42). □

The next result explains why the critical value $c=f_c(0)$ is the correct parameter-plane point at which to evaluate the dynamical Böttcher coordinate.

Proposition 4.2. *If $c\in\mathbb{C}\setminus\mathcal{M}$, then both 0 and $c=f_c(0)$ belong to the basin of infinity $A_c(\infty)$ from Definition* 3.2. *Moreover, the critical orbit eventually enters every sufficiently small neighbourhood of infinity. In particular, there exists an integer $N\ge 1$ such that $f_c^{\circ N}(0)\in U_c$, where U_c is the exterior neighbourhood on which the local Böttcher coordinate in Theorem 4.1 is defined.*

Proof. Assume that $c\notin\mathcal{M}$. By Definition 3.3, the critical orbit

$0, f_c(0) = c, f_c^{\circ 2}(0), \cdots$ is unbounded.

For a polynomial, an unbounded forward orbit necessarily tends to infinity. Indeed, the reverse triangle inequality gives

$$|f_c(z)| = |z^2 + c| \geq |z|^2 - |c|. \tag{48}$$

The estimate (48) shows that, once an orbit enters a sufficiently large exterior region, its modulus continues to increase. Consequently, $f_c^{\circ n}(0) \to \infty$ as $n \to \infty$. It follows that the critical point 0 does not belong to the filled Julia set K_c. Hence

$$0 \in A_c(\infty) = \mathbb{C} \setminus K_c. \tag{49}$$

Since $c = f_c(0)$, the forward orbit of c is the tail of the critical orbit:

$$c,\ f_c(c) = f_c^{\circ 2}(0),\ f_c^{\circ 2}(c) = f_c^{\circ 3}(0),\ \cdots \tag{50}$$

Therefore,

$$f_c^{\circ n}(c) = f_c^{\circ(n+1)}(0) \to \infty. \tag{51}$$

The limit (51) proves that the critical value $c = f_c(0)$ also belongs to $A_c(\infty)$. Finally, because $f_c^{\circ n}(0) \to \infty$, the critical orbit eventually enters the exterior neighbourhood U_c supplied by Theorem 4.1. Hence there exists $N \geq 1$ such that $f_c^{\circ N}(0) \in U_c$. □

***Remark* 4.3.** Proposition 4.2 shows that the critical value $c = f_c(0)$ belongs to the basin of infinity and that its forward orbit eventually enters the exterior neighbourhood U_c. It does not, however, imply that the critical value c itself lies in the particular neighbourhood U_c on which the local coordinate of Theorem 4.1 is initially defined. Moreover, Theorem 4.1 is a fixed-parameter statement and does not by itself establish holomorphic dependence of the Böttcher coordinate on c. These two issues are addressed by the family construction near infinity and by the classical Douady–Hubbard parameter uniformization stated below.

Notation 4.4 (Critical orbit Polynomials). For $c \in \mathbb{C}$, define

$$z_0(c) := 0,\ z_{n+1}(c) := z_n(c)^2 + c,\ n \geq 0. \tag{52}$$

Equivalently, the recurrence (52) gives

$$z_n(c) = f_c^{\circ n}(0). \tag{53}$$

For every $n \geq 1$, the function $c \mapsto z_n(c)$ is a polynomial in c. In particular,

$$z_1(c) = c,\ z_2(c) = c^2 + c,\ z_3(c) = (c^2 + c)^2 + c. \tag{54}$$

If $c \in \mathbb{C} \setminus \mathcal{M}$, then $z_n(c) \to \infty$ as $n \to \infty$ by Proposition 4.2.

Definition 4.5 (Local Parameter Böttcher Branch). Let $V \subset \mathbb{C} \setminus \mathcal{M}$ be a simply connected parameter domain. Suppose that $N \geq 1$ and $R > 1$ are such that $|z_N(c)| > R$ for $c \in V$, where $z_N(c) = f_c^{\circ N}(0)$.

Let $\phi : V \times \{z \in \mathbb{C} : |z| > R\} \to \mathbb{C}$ be the jointly holomorphic Böttcher coordinate supplied by Proposition 4.7. A *local parameter Böttcher branch* on V is a holomorphic function $\Phi_V : V \to \mathbb{C} \setminus \overline{\mathbb{D}}$, satisfying

$$\Phi_V(c)^{2^{N-1}} = \phi(c, z_N(c)),\ c \in V. \tag{55}$$

Equation (55) is understood with the root branch selected compatibly with the normalization (36).

Notation 4.6 (Normalized Critical orbit Root Approximants). On a simply connected parameter domain $V \subset \mathbb{C} \setminus \mathcal{M}$ where compatible holomorphic roots have been selected, write

$$\Phi_n(c) := z_n(c)^{1/2^{n-1}}, \quad n \geq 1. \tag{56}$$

The root expressions in (56) are understood locally through compatible holomorphic branches. This notation is local until the global parameter Böttcher map has been established by Theorem 4.8.

The following standard family version of the local Böttcher construction is included with proof in the notation required below; compare [1], Chapter VI and [5], Chapter 8.

Proposition 4.7 (Joint Holomorphic Dependence near Infinity). *Let $V \subset \mathbb{C}$ be a relatively compact parameter domain. Then there exists $R > 1$ and a jointly holomorphic function $\phi : V \times \{z \in \mathbb{C} : |z| > R\} \to \mathbb{C}$ such that, for every $c \in V$, the map $z \mapsto \phi_c(z) := \phi(c,z)$ is the normalized Böttcher coordinate of f_c on $\{|z| > R\}$. In particular, $\phi(c, f_c(z)) = \phi(c,z)^2$ whenever $|z| > R$, and $\dfrac{\phi(c,z)}{z} \to 1$ as $z \to \infty$, locally uniformly with respect to $c \in V$.*

Proof. Since V is relatively compact, its closure $\overline{V}$ is compact. Hence there exists $B > 0$ such that $|c| \leq B$ for every $c \in \overline{V}$, and therefore for every $c \in V$. Choose $R > 1$ sufficiently large that $R^2 - B > R$ and $\dfrac{B}{R^2} < \dfrac{1}{2}$. Then, for $c \in V$ and $|z| > R$,

$$|f_c(z)| = |z^2 + c| \geq |z|^2 - |c| > R. \tag{57}$$

Estimate (57) shows that the common exterior region $\{z \in \mathbb{C} : |z| > R\}$ is forward invariant under f_c for every $c \in V$. Consequently, for $c \in V$ and $|z| > R$, define $z_j(c,z) := f_c^{\circ j}(z)$. By (57),

$$|z_j(c,z)| > R, \quad j \geq 0. \tag{58}$$

For $c \in V$ and $|z| > R$, define

$$H(c,z) := \sum_{j=0}^{\infty} \frac{1}{2^{j+1}} \operatorname{Log}\left(1 + \frac{c}{z_j(c,z)^2}\right), \tag{59}$$

where Log denotes the branch of the logarithm defined near 1 and normalized by $\operatorname{Log} 1 = 0$.

Since $|c| \leq B$, the orbit estimate (58) and the choice $B/R^2 < 1/2$ give

$$\left|\frac{c}{z_j(c,z)^2}\right| \leq \frac{B}{R^2} < \frac{1}{2}, \quad j \geq 0. \tag{60}$$

Condition (60) ensures that every logarithmic term in (59) is evaluated in a common neighbourhood of 1. Moreover, the forward-invariance estimate (57) implies rapid growth of the iterates in the common exterior region. Consequently, the series in (59) converges locally uniformly on $V \times \{z \in \mathbb{C} : |z| > R\}$. Each summand is jointly holomorphic in (c, z), and therefore $H(c, z)$ is jointly holomorphic.

Define

$$\phi(c, z) := z \exp(H(c, z)). \tag{61}$$

Since H is jointly holomorphic, the definition (61) shows that ϕ is jointly holomorphic.

Separating the first term of the series (59) and using the recurrence $z_{j+1}(c, z) = z_j(c, f_c(z))$ gives

$$\phi(c, f_c(z)) = \phi(c, z)^2. \tag{62}$$

By (61), $\frac{\phi(c,z)}{z} = \exp(H(c, z))$. Since the series (59) tends locally uniformly to zero as $z \to \infty$, one obtains

$$\frac{\phi(c,z)}{z} \to 1 \ (z \to \infty), \tag{63}$$

locally uniformly with respect to $c \in V$.

For each fixed $c \in V$, the functional Equation (62) and the normalization (63), together with uniqueness in Theorem 4.1, show that $\phi(c, \cdot)$ is the normalized local Böttcher coordinate of f_c. □

Theorem 4.8 (Douady--Hubbard Parameter Uniformization; classical, see [2] [3], [4] Chapter 13, and [5] Chapter 14).
There exists a unique conformal isomorphism $\Phi_{\mathcal{M}} : \mathbb{C} \setminus \mathcal{M} \to \mathbb{C} \setminus \overline{\mathbb{D}}$ *satisfying the normalization* $\frac{\Phi_{\mathcal{M}}(c)}{c} \to 1$ *as* $c \to \infty$. *Let* $c_0 \in \mathbb{C} \setminus \mathcal{M}$. *Then there exist a simply connected neighbourhood* $V \subset \mathbb{C} \setminus \mathcal{M}$ *of* c_0, *an integer* $N \geq 1$, *and a number* $R > 1$ *such that* $|z_N(c)| > R$, $c \in V$ *where* $z_N(c) = f_c^{\circ N}(0)$ *is the critical orbit polynomial defined in Notation 4.4. Moreover, if* $\phi : V \times \{z \in \mathbb{C} : |z| > R\} \to \mathbb{C}$ *is the jointly holomorphic exterior Böttcher coordinate supplied by Proposition 4.7, then*

$$\Phi_{\mathcal{M}}(c)^{2^{N-1}} = \phi(c, z_N(c)), \ c \in V. \tag{64}$$

The relation (64) *identifies the restriction* $\Phi_{\mathcal{M}}|_V$ *with the local parameter Böttcher branch of Definition* 4.5 *that is compatible with the normalization at infinity. In particular,* $\Phi_{\mathcal{M}}$ *is holomorphic and nonvanishing on* $\mathbb{C} \setminus \mathcal{M}$, *and*

$$|\Phi_{\mathcal{M}}(c)| > 1, \ c \in \mathbb{C} \setminus \mathcal{M}. \tag{65}$$

Proof. The existence of the conformal isomorphism $\Phi_{\mathcal{M}} : \mathbb{C} \setminus \mathcal{M} \to \mathbb{C} \setminus \overline{\mathbb{D}}$, with the normalization (36), is the classical Douady–Hubbard external uniformization theorem for the quadratic connectedness locus.

We verify the stated local representation in the notation used in this paper. Fix

$c_0 \in \mathbb{C} \setminus \mathcal{M}$. By Proposition 4.2, and the critical orbit representation (53),

$$z_n(c_0) = f_{c_0}^{\circ n}(0) \to \infty \quad (n \to \infty). \tag{66}$$

Choose a relatively compact parameter neighbourhood $W \subset \mathbb{C} \setminus \mathcal{M}$ of c_0. By Proposition 4.7, there exist $R > 1$ and a jointly holomorphic function $\phi : W \times \{z \in \mathbb{C} : |z| > R\} \to \mathbb{C}$ such that, for each $c \in W$, the function $\phi_c(z) := \phi(c,z)$ is the normalized dynamical Böttcher coordinate of f_c on the common exterior region $\{|z| > R\}$. By Proposition 4.7, the map ϕ satisfies the functional Equation (62) and the normalization (63). Since $z_n(c_0) \to \infty$, there exists $N \ge 1$ such that $|z_N(c_0)| > R$. By Notation 4.4, $z_N(c)$ is a polynomial in c, and hence is holomorphic and continuous. After shrinking W to a sufficiently small simply connected neighbourhood V of c_0, we therefore have

$$|z_N(c)| > R, \ c \in V. \tag{67}$$

Define

$$F_N(c) := \phi(c, z_N(c)). \tag{68}$$

By (67), the composition in (68) is holomorphic on V. Moreover, because each ϕ_c is a Böttcher coordinate with values in $\mathbb{C} \setminus \overline{\mathbb{D}}$, the function F_N is nonvanishing on V.

Because the function F_N defined in (68) is nonvanishing on the simply connected domain V, it admits a holomorphic logarithm and, consequently, a holomorphic 2^{N-1}-st root. By Definition 4.5, the root branch compatible with the normalization at infinity defines Φ_V and satisfies (55).

The definition is independent of the chosen entry time. Indeed, if $m \ge N$, then

$$z_m(c) = f_c^{\circ(m-N)}(z_N(c)). \tag{69}$$

Repeated application of the functional Equation (62) along the orbit identity (69) gives

$$\phi(c, z_m(c)) = \phi(c, z_N(c))^{2^{m-N}}. \tag{70}$$

Therefore, for the compatible local root branches,

$$\phi(c, z_m(c))^{1/2^{m-1}} = \phi(c, z_N(c))^{1/2^{N-1}}. \tag{71}$$

Identity (71) proves that the normalized pullback is unchanged when a later entry time is used.

The classical Douady–Hubbard theorem guarantees that the normalized local branches obtained in this manner are compatible on overlaps and patch together to form a single-valued holomorphic map on $\mathbb{C} \setminus \mathcal{M}$. This global map is precisely $\Phi_{\mathcal{M}}$. Consequently, the globally defined parameter Böttcher map satisfies the local representation (64) on V.

The same classical theorem establishes that $\Phi_{\mathcal{M}}$ is one-to-one and maps $\mathbb{C} \setminus \mathcal{M}$ onto $\mathbb{C} \setminus \overline{\mathbb{D}}$. Therefore $\Phi_{\mathcal{M}}$ is a conformal isomorphism. Since $\Phi_{\mathcal{M}}$

maps $\mathbb{C}\setminus\mathcal{M}$ onto $\mathbb{C}\setminus\overline{\mathbb{D}}$, the modulus estimate (65) follows.

It remains to prove uniqueness under the stated normalization. Suppose that $\Psi:\mathbb{C}\setminus\mathcal{M}\to\mathbb{C}\setminus\overline{\mathbb{D}}$ is another conformal isomorphism satisfying the normalization $\Psi(c)/c\to 1$ as $c\to\infty$, analogous to (36). Then $A:=\Psi\circ\Phi_{\mathcal{M}}^{-1}$ is an automorphism of $\mathbb{C}\setminus\overline{\mathbb{D}}$ that fixes infinity. Every such automorphism is a rotation, $A(w)=\mathrm{e}^{i\theta}w$. The normalization at infinity gives $\mathrm{e}^{i\theta}=1$. Hence A is the identity map, and therefore $\Psi=\Phi_{\mathcal{M}}$. □

Corollary 4.9 (Critical Orbit Representation). *Let* $V\subset\mathbb{C}\setminus\mathcal{M}$ *be a simply connected parameter neighbourhood on which the compatible holomorphic root branches are chosen according to Definition* 4.5. *Then*

$$\Phi_{\mathcal{M}}(c)=\lim_{n\to\infty} z_n(c)^{1/2^{n-1}}, \tag{72}$$

locally uniformly for $c\in V$. Equivalently,

$$\Phi_{\mathcal{M}}(c)=\lim_{n\to\infty}\left(f_c^{\circ n}(0)\right)^{1/2^{n-1}}. \tag{73}$$

where the roots denote the local holomorphic branches compatible with the normalization (36).

Proof. Let N and R be as in Theorem 4.8. For $n\ge N$, the orbit point $z_n(c)$ lies in the common exterior Böttcher region. Since

$$\phi(c,z)=z(1+o(1))\ \ (z\to\infty), \tag{74}$$

locally uniformly with respect to c, applying (74) along the escaping critical orbit gives

$$\frac{\phi(c,z_n(c))}{z_n(c)}\to 1\ \ (n\to\infty), \tag{75}$$

locally uniformly on V. By the functional equation and Theorem 4.8,

$$\phi(c,z_n(c))=\Phi_{\mathcal{M}}(c)^{2^{n-1}}. \tag{76}$$

Consequently,

$$z_n(c)^{1/2^{n-1}}=\Phi_{\mathcal{M}}(c)\left(\frac{z_n(c)}{\phi(c,z_n(c))}\right)^{1/2^{n-1}}. \tag{77}$$

By (75), the second factor in (77) converges locally uniformly to 1. Hence the convergence asserted in (72) follows. □

***Remark* 4.10.** The root-limit formula in Corollary 4.9 is not used as a branch-free global definition of $\Phi_{\mathcal{M}}$. For arbitrary root choices, the expressions $z_n(c)^{1/2^{n-1}}$ are multivalued and do not by themselves establish either single-valuedness or holomorphic dependence on c. The global single-valued holomorphic map $\Phi_{\mathcal{M}}$ is supplied by the classical Douady–Hubbard uniformization theorem. The corollary expresses this already-established map locally through the uniquely compatible holomorphic root branches determined by its normalization at infinity.

***Remark* 4.11.** The notation $\Phi_{\mathcal{M}}(c)=\phi_c(c)$ is commonly used as shorthand for the classical identification between the parameter Böttcher map and the normalized dynamical exterior coordinate evaluated along the escaping critical orbit. It must not be interpreted as a direct evaluation of the local map supplied by Theorem 4.1, because the critical value c need not belong to the particular neighbourhood U_c on which that local coordinate is initially defined. More precisely, if $N \ge 1$ is chosen so that $z_N(c)=f_c^{\circ N}(0)$ lies in the exterior Böttcher region, then

$$\Phi_{\mathcal{M}}(c)^{2^{N-1}}=\phi_c(z_N(c)). \tag{78}$$

with the root selected by the normalization at infinity. Consequently,

$$\log\left|\Phi_{\mathcal{M}}(c)\right|=\frac{1}{2^{N-1}}\log\left|\phi_c(z_N(c))\right|. \tag{79}$$

Taking absolute values and logarithms in (78) gives (79). By the local Green-function identity (42), evaluated at $z_N(c)$,

$$g_c(z_N(c))=\log\left|\phi_c(z_N(c))\right|. \tag{80}$$

Combining (79), (80), and the dynamical functional Equation (32) gives

$$\log\left|\Phi_{\mathcal{M}}(c)\right|=g_c(c)=2g_c(0). \tag{81}$$

The geometric content of Theorem 4.8 is summarized in Figure 1. The exterior coordinate sends equipotentials to concentric circles and parameter external rays to radial half-lines.

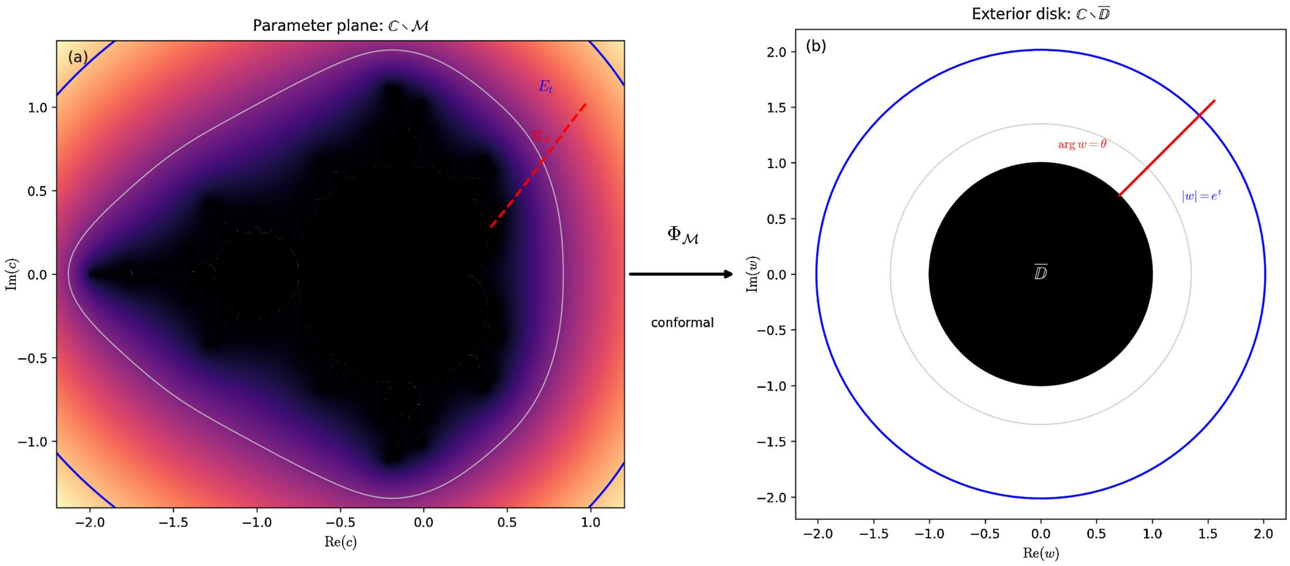

Figure 1. Schematic representation of the classical Douady–Hubbard exterior uniformization. By Theorem 4.8, the parameter Böttcher map $\Phi_{\mathcal{M}}$ conformally identifies $\mathbb{C}\setminus\mathcal{M}$ with $\mathbb{C}\setminus\overline{\mathbb{D}}$. Under this map, the equipotential $G_{\mathcal{M}}(c)=t$, defined using Definition 5.1, corresponds to the circle $|w|=\mathrm{e}^t$, as stated in Proposition 7.2. The parameter external ray of angle θ, introduced in Definition 7.1, corresponds to the radial half-line $w=r\mathrm{e}^{2\pi\mathrm{i}\theta}$, $r>1$. The parameter-plane ray is schematic and is included to illustrate the conformal correspondence rather than to represent a numerically computed inverse Böttcher ray.

5. Explicit Construction of the Green Function

We now construct the Green function of $\mathbb{C}\setminus\mathcal{M}$ explicitly from the parameter Böttcher map of Notation 3.11 and Theorem 4.8. The results of this section are classical consequences of the Douady-Hubbard parameter uniformization and standard logarithmic potential theory; see [1], Chapter VI, [2] [3], [5], Chapter 14, and [9]. They are included with proofs to fix the precise normalization used in the quantitative analysis.

Definition 5.1 (Exterior Green function). Let $\Phi_{\mathcal{M}}:\mathbb{C}\setminus\mathcal{M}\to\mathbb{C}\setminus\overline{\mathbb{D}}$ be the normalized parameter Böttcher map from Theorem 4.8. Define

$$G_{\mathcal{M}}(c):=\log\left|\Phi_{\mathcal{M}}(c)\right|,\quad c\in\mathbb{C}\setminus\mathcal{M}. \tag{82}$$

Equation (82) is the exact conformal definition used throughout the remainder of the paper.

***Remark* 5.2.** Definition 5.1 is the classical conformal representation of the exterior Green function:

$$G_{\mathcal{M}}=\log|\cdot|\circ\Phi_{\mathcal{M}}. \tag{83}$$

The composition formula (83) shows that $G_{\mathcal{M}}$ is defined exactly on $\mathbb{C}\setminus\mathcal{M}$, rather than only through its asymptotic behaviour at infinity.

We next identify this parameter-plane function with the dynamical Green function evaluated at the critical value.

Proposition 5.3. *For every* $c\in\mathbb{C}\setminus\mathcal{M}$, $G_{\mathcal{M}}(c)=g_c(c)$.

Proof. Fix $c\in\mathbb{C}\setminus\mathcal{M}$, and write $z_n(c)=f_c^{\circ n}(0)$. Choose $N\geq 1$ so that $z_N(c)$ belongs to an exterior neighbourhood on which the dynamical Böttcher coordinate ϕ_c is defined. By Theorem 4.8, the local representation (64),

$$\Phi_{\mathcal{M}}(c)^{2^{N-1}}=\phi_c\left(z_N(c)\right). \tag{84}$$

Taking absolute values and logarithms in (84) gives

$$\log\left|\Phi_{\mathcal{M}}(c)\right|=\frac{1}{2^{N-1}}\log\left|\phi_c\left(z_N(c)\right)\right|. \tag{85}$$

By Theorem 4.1, and the local identity (42),

$$\log\left|\phi_c\left(z_N(c)\right)\right|=g_c\left(z_N(c)\right). \tag{86}$$

Since the critical value is $c=f_c(0)$, one has

$$z_N(c)=f_c^{\circ(N-1)}(c). \tag{87}$$

Repeated application of the functional Equation (32) along (87) gives

$$g_c\left(z_N(c)\right)=2^{N-1}g_c(c). \tag{88}$$

Combining (85), (86), and (88) yields

$$\log\left|\Phi_{\mathcal{M}}(c)\right|=g_c(c). \tag{89}$$

Using Definition 5.1 and (82), we obtain $G_{\mathcal{M}}(c)=g_c(c)$. □

Corollary 5.4. *For every* $c \in \mathbb{C} \setminus \mathcal{M}$, $G_{\mathcal{M}}(c) = 2g_c(0)$. *Consequently,*

$$G_{\mathcal{M}}(c) = 2\lim_{n\to\infty} \frac{1}{2^n} \log^+ \left| f_c^{\circ n}(0) \right|. \tag{90}$$

Proof. Since $c = f_c(0)$, the functional Equation (32) from *Remark* 3.7 gives

$$g_c(c) = g_c(f_c(0)) = 2g_c(0). \tag{91}$$

Using Proposition 5.3, we conclude that $G_{\mathcal{M}}(c) = 2g_c(0)$. The limit formula (90) then follows from Definition 3.5 and (28), evaluated at $z = 0$. □

***Remark* 5.5.** Corollary 5.4 is the precise normalization bridge between the present paper and [6]. The earlier quantitative paper studied the critical-point regularization $g_c(0)$, whereas the present paper is organized around the parameter-plane Green function $G_{\mathcal{M}}(c) = g_c(c)$. The factor 2 reflects the single-step passage from the critical point 0 to the critical value $c = f_c(0)$.

Proposition 5.6. *The function* $G_{\mathcal{M}}$ *is harmonic on* $\mathbb{C} \setminus \mathcal{M}$.

Proof. By Theorem 4.8, the map $\Phi_{\mathcal{M}}$ is holomorphic and maps $\mathbb{C} \setminus \mathcal{M}$ into $\mathbb{C} \setminus \overline{\mathbb{D}}$. In particular, $\Phi_{\mathcal{M}}$ is nowhere zero on $\mathbb{C} \setminus \mathcal{M}$. Hence, near every point of $\mathbb{C} \setminus \mathcal{M}$, one may choose a holomorphic branch of $\operatorname{Log} \Phi_{\mathcal{M}}$. On such a neighbourhood,

$$\log|\Phi_{\mathcal{M}}| = \operatorname{Re}(\operatorname{Log} \Phi_{\mathcal{M}}). \tag{92}$$

Identity (92) shows that $\log|\Phi_{\mathcal{M}}|$ is harmonic locally. Since harmonicity is a local property and $G_{\mathcal{M}} = \log|\Phi_{\mathcal{M}}|$ by Definition 5.1 and (82), $G_{\mathcal{M}}$ is harmonic on $\mathbb{C} \setminus \mathcal{M}$. □

Proposition 5.7. *For every* $c \in \mathbb{C} \setminus \mathcal{M}$, *one has* $G_{\mathcal{M}}(c) > 0$.

Proof. If $c \in \mathbb{C} \setminus \mathcal{M}$, then Theorem 4.8 gives $\Phi_{\mathcal{M}}(c) \in \mathbb{C} \setminus \overline{\mathbb{D}}$. The modulus estimate (65) gives $|\Phi_{\mathcal{M}}(c)| > 1$. Taking logarithms and using Definition 5.1 together with (82) gives $G_{\mathcal{M}}(c) > 0$. □

Theorem 5.8 (Logarithmic growth at infinity). *As* $c \to \infty$,

$$G_{\mathcal{M}}(c) - \log|c| \to 0. \tag{93}$$

Proof. By Theorem 4.8 and the normalization (36), $\dfrac{\Phi_{\mathcal{M}}(c)}{c} \to 1$ as $c \to \infty$. Taking moduli gives

$$\left| \frac{\Phi_{\mathcal{M}}(c)}{c} \right| \to 1 \ (c \to \infty). \tag{94}$$

Since the real logarithm is continuous at 1, it follows that

$$\log\left| \frac{\Phi_{\mathcal{M}}(c)}{c} \right| = \log|\Phi_{\mathcal{M}}(c)| - \log|c| \to 0. \tag{95}$$

Using (82) in (95) gives (93). □

Corollary 5.9. *The function* $G_{\mathcal{M}}$ *has a logarithmic pole at infinity in the sense of Definition* 3.8.

Proof. By Theorem 5.8 and (93), $G_{\mathcal{M}}(c) = \log|c| + o(1)$ as $c \to \infty$, which is exactly the normalization in Definition 3.8 and (33). □

Proposition 5.10. *The function* $G_{\mathcal{M}}$ *extends continuously to* $\mathbb{C}$ *by setting* $G_{\mathcal{M}}(c)=0$ *for all* $c\in\mathcal{M}$. *In particular,* $G_{\mathcal{M}}=0$ *on* $\partial\mathcal{M}$.

Proof. By Corollary 5.4, $G_{\mathcal{M}}(c)=2g_c(0)$ for all $c\in\mathbb{C}\setminus\mathcal{M}$. The escape-rate function $(c,z)\mapsto g_c(z)$ is continuous for the quadratic family; see, for example, [1], Chapter VI, or [5], Chapter 8. In particular, the function $c\mapsto g_c(0)$ is continuous on $\mathbb{C}$. Moreover,

$$g_c(0)=0 \iff 0\in K_c \iff c\in\mathcal{M}. \tag{96}$$

Let $c_j\in\mathbb{C}\setminus\mathcal{M}$ and suppose that $c_j\to c_*\in\partial\mathcal{M}$. By continuity,

$$G_{\mathcal{M}}(c_j)=2g_{c_j}(0)\to 2g_{c_*}(0)=0. \tag{97}$$

The final equality in (97) follows from (96), since $c_*\in\partial\mathcal{M}\subset\mathcal{M}$. Define

$$G_{\mathcal{M}}(c):=0,\ \ c\in\mathcal{M}. \tag{98}$$

The convergence (97) shows that the extension (98) is continuous on all of $\mathbb{C}$. In particular, $G_{\mathcal{M}}=0$ on $\partial\mathcal{M}$. □

Theorem 5.11 (Structural Characterization of $G_{\mathcal{M}}$). *The function* $G_{\mathcal{M}}$ *constructed in Definition* 5.1 *has the following properties*:

(i) $G_{\mathcal{M}}$ is harmonic on $\mathbb{C}\setminus\mathcal{M}$;

(ii) $G_{\mathcal{M}}(c)>0$ for every $c\in\mathbb{C}\setminus\mathcal{M}$;

(iii) $G_{\mathcal{M}}$ extends continuously to $\mathbb{C}$ and vanishes on $\mathcal{M}$;

(iv) $G_{\mathcal{M}}(c)-\log|c|\to 0$ as $c\to\infty$.

Proof. Part (i) is Proposition 5.6. Part (ii) is Proposition 5.7. Part (iii) is Proposition 5.10. Part (iv) is Theorem 5.8, equivalently the logarithmic-pole normalization of Definition 3.8. □

6. Uniqueness of the Exterior Green Function

We now prove the classical uniqueness characterization of $G_{\mathcal{M}}$ as the Green function of $\mathbb{C}\setminus\mathcal{M}$ with pole at infinity in the normalization of Definition 3.8; compare [9] and [10]. The proof is included for completeness.

Theorem 6.1 (Uniqueness of the Normalized Exterior Green Function) *Let* $u:\mathbb{C}\setminus\mathcal{M}\to\mathbb{R}$ *be a function satisfying*:

(a) u is harmonic on $\mathbb{C}\setminus\mathcal{M}$;

(b) u extends continuously to $\partial\mathcal{M}$ and $u=0$ on $\partial\mathcal{M}$;

(c) u has a logarithmic pole at infinity with the normalization of Definition 3.8, namely the condition (33).

Then $u(c)=G_{\mathcal{M}}(c)$ *for every* $c\in\mathbb{C}\setminus\mathcal{M}$.

Proof. Define

$$h(c):=u(c)-G_{\mathcal{M}}(c),\ \ c\in\mathbb{C}\setminus\mathcal{M}. \tag{99}$$

By the harmonicity of u and Proposition 5.6, the function h defined in (99) is harmonic on $\mathbb{C}\setminus\mathcal{M}$.

By the boundary condition on u and Proposition 5.10, the function h extends continuously to $\partial\mathcal{M}$ and satisfies $h=0$ on $\partial\mathcal{M}$. Furthermore, by the growth assumption on u, Theorem 5.8, and (93),

$$h(c)=\left(u(c)-\log|c|\right)-\left(G_{\mathcal{M}}(c)-\log|c|\right)\to 0\quad (c\to\infty). \tag{100}$$

Fix $c_0\in\mathbb{C}\setminus\mathcal{M}$. Since $\mathcal{M}$ is compact, choose $R_0>0$ such that $\mathcal{M}\subset\{|c|<R_0\}$. For $R>R_0$ with $|c_0|<R$, set

$$\Omega_R:=\{c\in\mathbb{C}\setminus\mathcal{M}:|c|<R\}. \tag{101}$$

The function h is harmonic on Ω_R, continuous up to the boundary pieces $\partial\mathcal{M}$ and $\{|c|=R\}$, and the boundary of Ω_R is contained in

$$\partial\Omega_R\subset\partial\mathcal{M}\cup\{c\in\mathbb{C}:|c|=R\}. \tag{102}$$

Set

$$\varepsilon(R):=\sup_{|c|=R}|h(c)|. \tag{103}$$

By (100), $\varepsilon(R)\to 0$ as $R\to\infty$. The maximum principle applied to both h and $-h$ on Ω_R gives

$$|h(c)|\le\max\left\{\sup_{\partial\mathcal{M}}|h|,\sup_{|c|=R}|h|\right\}=\varepsilon(R),\ \ c\in\Omega_R. \tag{104}$$

Applying (104) at $c=c_0$ gives $|h(c_0)|\le\varepsilon(R)$. Letting $R\to\infty$ and using $\varepsilon(R)\to 0$, which follows from (100), gives $h(c_0)=0$. Since $c_0\in\mathbb{C}\setminus\mathcal{M}$ was arbitrary, it follows that $h\equiv 0$ on $\mathbb{C}\setminus\mathcal{M}$. Therefore, $u=G_{\mathcal{M}}$ on $\mathbb{C}\setminus\mathcal{M}$. □

Corollary 6.2. *The function* $G_{\mathcal{M}}$ *is the normalized Green function of* $\mathbb{C}\setminus\mathcal{M}$ *with pole at infinity. Moreover, it is unique among functions satisfying the hypotheses of Theorem* 6.1.

Proof. By Theorem 5.8 and (93), the function $G_{\mathcal{M}}$ has the normalization required by Definition 3.8 and (33). Thus $G_{\mathcal{M}}$ satisfies the existence properties required of the normalized Green function on $\mathbb{C}\setminus\mathcal{M}$.

If $u:\mathbb{C}\setminus\mathcal{M}\to\mathbb{R}$ is any other function with the same normalization at infinity and satisfying the hypotheses of Theorem 6.1, then Theorem 6.1 gives $u=G_{\mathcal{M}}$ on $\mathbb{C}\setminus\mathcal{M}$. This proves uniqueness. □

Remark **6.3.** The proof of Theorem 6.1 is an unbounded-domain uniqueness argument. The difference of two admissible Green functions is harmonic, vanishes on the inner boundary, tends to zero on the outer boundary at infinity, and is therefore forced to vanish identically by an exhaustion of the domain and the maximum principle.

7. Equipotentials and External Geometry

The conformal representation (82) from Definition 5.1 makes the geometry of the Mandelbrot exterior transparent. The following standard equipotential and external-ray conventions are induced by the parameter Böttcher coordinate; see [2] [3], [4] Chapter 13, and [5] Chapter 14.

Definition 7.1 (Equipotentials and External Rays). For $t > 0$, the equipotential of level t is

$$E_t := \{c \in \mathbb{C} \setminus \mathcal{M} : G_{\mathcal{M}}(c) = t\}, \quad t > 0. \tag{105}$$

For $\theta \in \mathbb{R}/\mathbb{Z}$, the parameter external ray of angle θ, measured in turns, is

$$\mathcal{R}_\theta := \Phi_{\mathcal{M}}^{-1}\left(\{re^{2\pi i\theta} : r > 1\}\right), \quad \theta \in \mathbb{R}/\mathbb{Z}. \tag{106}$$

Proposition 7.2. *For every* $t > 0$, $E_t = \Phi_{\mathcal{M}}^{-1}(C_t)$, *where* C_t *is the exterior circle defined in* (38) *and Notation* 3.13.

Proof. Let $t > 0$, and let $c \in \mathbb{C} \setminus \mathcal{M}$. By Definition 7.1, Definition 5.1, and Notation 3.13, together with (105), (82), and (38), one has

$$\begin{aligned} c \in E_t &\Leftrightarrow G_{\mathcal{M}}(c) = t \\ &\Leftrightarrow \log\left|\Phi_{\mathcal{M}}(c)\right| = t \\ &\Leftrightarrow \left|\Phi_{\mathcal{M}}(c)\right| = e^t \\ &\Leftrightarrow \Phi_{\mathcal{M}}(c) \in C_t. \end{aligned} \tag{107}$$

The equivalence chain (107) proves $E_t = \Phi_{\mathcal{M}}^{-1}(C_t)$. □

***Remark* 7.3.** Proposition 7.2 shows that the equipotentials of the Mandelbrot set are obtained by pulling back Euclidean circles under the exterior conformal map $\Phi_{\mathcal{M}}$. Thus the level sets of $G_{\mathcal{M}}$ are the geometric traces of the uniformization $\mathbb{C} \setminus \mathcal{M} \cong \mathbb{C} \setminus \overline{\mathbb{D}}$.

***Remark* 7.4.** The equipotentials E_t and the external rays $\mathcal{R}_\theta$, introduced in Definition 7.1, are the two basic foliations induced by the exterior conformal coordinate. In the w-plane, the sets $|w| = \text{constant}$ and $\arg w = \text{constant}$ are orthogonal. Their pullbacks through $\Phi_{\mathcal{M}}$ encode the external geometry of the Mandelbrot set in a conformally natural way.

Observation 7.5. The positivity of $G_{\mathcal{M}}$ on $\mathbb{C} \setminus \mathcal{M}$, proved in Proposition 5.7, together with the identity $G_{\mathcal{M}} = 0$ on $\mathcal{M}$, proved in Proposition 5.10, shows that $\mathcal{M}$ is the zero-level set of the Green function. In this sense, the Mandelbrot set is the natural equipotential boundary of its own exterior domain.

8. Quantitative Approximation of the Parameter Böttcher Potential

In the author's earlier work [6], the finite critical orbit escape rate approximants of Definition 3.6 were studied quantitatively, with explicit convergence estimates in the escaping regime. In the present paper, the structurally natural parameter-space Green function is identified by Proposition 5.3 and the conformal–dynamical identity (89) as $G_{\mathcal{M}}(c) = \log\left|\Phi_{\mathcal{M}}(c)\right| = g_c(c)$. The quantitative estimate in the following theorem was established in the author's earlier work [6]. The present formulation provides a self-contained telescoping derivation and identifies the estimate with approximation of the parameter Böttcher potential through the conformal-dynamical normalization (81).

Theorem 8.1 (Quantitative--Conformal Bridge Theorem). *Let* $c \in \mathbb{C} \setminus \mathcal{M}$, *and let* $G_n(c)$ *be the finite critical orbit escape rate approximants from Definition* 3.6. *Assume that, for some* $n_0 \in \mathbb{N}$, *there exists an escape radius* $R > \max\{2, \sqrt{2|c|}\}$ *such that* $|f_c^{\circ n_0}(0)| \geq R$. *Then, for every* $n \geq n_0$,

$$\left|2G_n(c) - \log|\Phi_{\mathcal{M}}(c)|\right| \leq \frac{2}{2^n}\left[-\log\left(1 - \frac{|c|}{R^2}\right)\right]. \tag{108}$$

In particular,

$$2G_n(c) \to \log|\Phi_{\mathcal{M}}(c)| \quad (n \to \infty), \tag{109}$$

with explicit exponential error control of order $O(2^{-n})$.

Proof. Set $z_n := f_c^{\circ n}(0)$ where $n \geq 0$. Since $c \in \mathbb{C} \setminus \mathcal{M}$, the critical orbit of f_c escapes to infinity by Definition 3.3. By Definitions 3.5 and 3.6, together with (31), one has $G_n(c) \to g_c(0)$. By Corollary 5.4, and the identity (81) $\log|\Phi_{\mathcal{M}}(c)| = G_{\mathcal{M}}(c) = 2g_c(0)$. By hypothesis, $|z_{n_0}| \geq R$, where $R > \max\{2, \sqrt{2|c|}\}$. In particular, $0 \leq \frac{|c|}{R^2} < \frac{1}{2}$. We first show that the orbit remains in the escape region after time n_0. Suppose that $|z_k| \geq R$ for some $k \geq n_0$. Then

$$|z_{k+1}| = |z_k^2 + c| \geq |z_k|^2 - |c|. \tag{110}$$

Since $R^2 > 2|c|$ and $|z_k| \geq R$, one has $|c| < R^2/2 \leq |z_k|^2/2$. Combining this with (110) gives

$$|z_{k+1}| \geq \frac{|z_k|^2}{2} \geq |z_k| \geq R. \tag{111}$$

By induction from (111),

$$|z_k| \geq R, \quad k \geq n_0. \tag{112}$$

For every $k \geq n_0$, the critical orbit recurrence (29) may be written in the factorized form

$$z_{k+1} = z_k^2 + c = z_k^2\left(1 + \frac{c}{z_k^2}\right). \tag{113}$$

Since (112) gives $|z_k| \geq R > 2$, the positive logarithm agrees with the ordinary logarithm. Using (30) and (113), one obtains

$$\begin{aligned} G_{k+1}(c) - G_k(c) &= \frac{1}{2^{k+1}}\log|z_{k+1}| - \frac{1}{2^k}\log|z_k| \\ &= \frac{1}{2^{k+1}}\log\left|1 + \frac{c}{z_k^2}\right|. \end{aligned} \tag{114}$$

Let $m > n \geq n_0$. Summing (114) from $k = n$ to $m - 1$ gives

$$G_m(c) - G_n(c) = \sum_{k=n}^{m-1}\frac{1}{2^{k+1}}\log\left|1 + \frac{c}{z_k^2}\right|. \tag{115}$$

Letting $m \to \infty$ in (115) and using (31), one obtains

$$g_c(0) - G_n(c) = \sum_{k=n}^{\infty} \frac{1}{2^{k+1}} \log\left|1 + \frac{c}{z_k^2}\right|. \tag{116}$$

For $k \ge n_0$, the orbit bound (112) gives

$$\left|\frac{c}{z_k^2}\right| \le \frac{|c|}{R^2} < 1. \tag{117}$$

For every $u \in \mathbb{C}$ satisfying $|u| < 1$,

$$1 - |u| \le |1 + u| \le 1 + |u|. \tag{118}$$

Consequently,

$$\big|\log|1 + u|\big| \le -\log(1 - |u|). \tag{119}$$

The modulus bounds (118) imply the logarithmic estimate (119). Applying (119) with $u = c/z_k^2$, and then using (112), gives

$$\begin{aligned} \left|\log\left|1 + \frac{c}{z_k^2}\right|\right| &\le -\log\left(1 - \frac{|c|}{|z_k|^2}\right) \\ &\le -\log\left(1 - \frac{|c|}{R^2}\right). \end{aligned} \tag{120}$$

Combining (116) and (120) yields

$$\begin{aligned} |g_c(0) - G_n(c)| &\le \sum_{k=n}^{\infty} \frac{1}{2^{k+1}} \left[-\log\left(1 - \frac{|c|}{R^2}\right)\right] \\ &= \frac{1}{2^n}\left[-\log\left(1 - \frac{|c|}{R^2}\right)\right]. \end{aligned} \tag{121}$$

Finally, multiplying (121) by 2 and using Corollary 5.4 together with (81) gives the claimed bound (108). The factor $-\log\left(1 - |c|/R^2\right)$ is finite and independent of n. Therefore, the right-hand side of (108) tends to zero at the rate $O\left(2^{-n}\right)$, proving (109). □

***Remark* 8.2 (Interpretation of the Quantitative Estimate).** Theorem 8.1 separates the approximation error into the geometric decay factor 2^{-n} and an escape-region constant. Define

$$C(c, R) := 2\left[-\log\left(1 - \frac{|c|}{R^2}\right)\right]. \tag{122}$$

With the constant in (122), the bound (108) may be written as $\big|2G_n(c) - \log|\Phi_{\mathcal{M}}(c)|\big| \le C(c, R)2^{-n}$. For fixed c and R, the constant $C(c, R)$ is independent of n. Thus, once the critical orbit has entered the escape region $\{z \in \mathbb{C} : |z| \ge R\}$, the remaining approximation error decreases geometrically at the rate 2^{-n}. The condition $R > \max\left\{2, \sqrt{2|c|}\right\}$ has two roles. First, the inequality $R > \sqrt{2|c|}$ ensures that $|c|/R^2 < 1/2$, so the logarithmic correction terms are uniformly controlled. Second, the inequality $R > 2$, together with the forward-invariance estimate (111), ensures that the critical orbit remains in the escape region after its first entry. Consequently, the estimate (108) applies for every $n \ge n_0$. The telescoping argument is included to make the proof self-contained. Although the underlying escape-rate estimate was established in [6], the present theorem identifies its parameter-plane conformal meaning through the classical identity (81).

Corollary 8.3. *For every escaping parameter* $c \in \mathbb{C} \setminus \mathcal{M}$*, the finite escape-rate approximants* $2G_n(c)$ *provide an explicit quantitative approximation to the parameter Böttcher potential* $\log|\Phi_{\mathcal{M}}(c)|$.

Proof. Let $c \in \mathbb{C} \setminus \mathcal{M}$. Since c is escaping, the critical orbit eventually enters an escape region. Thus, there exist $n_0 \in \mathbb{N}$ and $R > \max\{2, \sqrt{2|c|}\}$ such that

$$\left|f_c^{\circ n_0}(0)\right| \ge R. \tag{123}$$

Applying Theorem 8.1 under the entry condition (123), one obtains the estimate (108) for every $n \ge n_0$. The constant $C(c, R)$ defined in (122) is finite and independent of n. Hence the right-hand side tends to 0 as $n \to \infty$. Consequently, the convergence (109) holds. Moreover, (108) provides an explicit error bound at every finite step $n \ge n_0$, so the approximation is quantitative. □

The pointwise estimate has the following compact-uniform consequence, developed in the present manuscript.

Corollary 8.4 (Uniform Quantitative Approximation on Compacta). *Let* $K \subset \mathbb{C} \setminus \mathcal{M}$ *be a nonempty compact set. Then there exist an integer* $n_K \ge 1$ *and a constant* $C_K > 0$ *such that*

$$\sup_{c \in K}\left|2G_n(c) - G_{\mathcal{M}}(c)\right| \le C_K 2^{-n}, \quad n \ge n_K. \tag{124}$$

Equivalently, $2G_n \to G_{\mathcal{M}}$ locally uniformly on $\mathbb{C} \setminus \mathcal{M}$, with exponential rate on every compact subset.

Proof. Since K is nonempty and compact, define

$$M_K := \max_{c \in K}|c|. \tag{125}$$

The number M_K is finite. Choose $R_K > 0$ such that

$$R_K > \max\left\{2, \sqrt{2M_K}\right\}. \tag{126}$$

Since $|c| \le M_K$ for every $c \in K$, (126) implies that $R_K > \max\{2, \sqrt{2|c|}\}$ for every $c \in K$. Thus, R_K satisfies the escape-radius condition in Theorem 8.1 uniformly over K. For each $c \in K$, the critical orbit defined in Notation 4.4 escapes because $c \notin \mathcal{M}$. Hence there exists an integer $n(c) \ge 1$ such that

$$\left|z_{n(c)}(c)\right| > R_K. \tag{127}$$

By Notation 4.4, the map $c' \mapsto z_{n(c)}(c')$ is a polynomial and is therefore continuous. Consequently, the strict inequality in (127) persists on a sufficiently small open neighbourhood V_c of c. Thus,

$$\left|z_{n(c)}(c')\right| > R_K, \quad c' \in V_c. \tag{128}$$

The family $\{V_c : c \in K\}$ is an open cover of K. By compactness, there exist $c_1, \cdots, c_m \in K$ such that $K \subset V_{c_1} \cup \cdots \cup V_{c_m}$. Define

$$n_K := \max_{1 \le j \le m} n(c_j). \tag{129}$$

Let $c \in K$. Choose $j \in \{1, \cdots, m\}$ such that $c \in V_{c_j}$. By (128), $\left|z_{n(c_j)}(c)\right| > R_K$. The forward-invariance estimate (111), proved in Theorem 8.1, shows that once the critical orbit enters the region $\{|z| > R_K\}$, it remains in that region. Since $n_K \ge n(c_j)$, it follows that

$$\left|z_{n_K}(c)\right| > R_K, \quad c \in K. \tag{130}$$

Define

$$C_K := 2\left[-\log\left(1 - \frac{M_K}{R_K^2}\right)\right]. \tag{131}$$

By (126), $0 \le \frac{M_K}{R_K^2} < \frac{1}{2}$. Therefore, the logarithm in (131) is well defined, and C_K is finite and positive. By (130), the hypotheses of Theorem 8.1 hold for every $c \in K$ and every $n \ge n_K$, with the common radius R_K. Using the conformal representation (82), the estimate (108) becomes an estimate for $\left|2G_n(c) - G_{\mathcal{M}}(c)\right|$. Moreover, the function $x \mapsto -\log(1-x)$ is increasing on $[0,1)$. Since $|c| \le M_K$, we therefore obtain

$$\begin{aligned}\left|2G_n(c) - G_{\mathcal{M}}(c)\right| &\le \frac{2}{2^n}\left[-\log\left(1 - \frac{|c|}{R_K^2}\right)\right] \\ &\le \frac{2}{2^n}\left[-\log\left(1 - \frac{M_K}{R_K^2}\right)\right] \\ &= C_K 2^{-n}.\end{aligned} \tag{132}$$

Taking the supremum over $c \in K$ in (132) gives (124).

□

***Remark* 8.5.** Corollary 8.4 strengthens the pointwise convergence in Theorem 8.1 to locally uniform convergence on $\mathbb{C} \setminus \mathcal{M}$. The compactness assumption is essential for obtaining a common escape radius, entry index, and error constant. No corresponding global uniform estimate is asserted near $\partial\mathcal{M}$.

8.1. Numerical Approximation Schemes and Visualization Methodology

The numerical visualizations in this paper are finite-resolution illustrations of the analytic objects constructed above. They are not used as substitutes for the proofs. Their purpose is to display, in finite-iteration form, the conformal and potential-theoretic structures described by Theorem 4.8, Definition 5.1, Proposition 7.2, and Theorem 8.1.

Corollary 8.4, together with the compact-uniform estimate (124), shows that the fixed-index approximants converge uniformly and exponentially on compact subsets of the Mandelbrot exterior. This provides the analytic justification for using common finite iteration depths on compact positive-potential regions.

The computations use two related numerical regimes. The first is based on finite critical orbit approximants, as introduced in Definition 3.6. This regime is used for the parameter-plane Green-function heat map, the convergence plot, and the equipotential-stability visualization. The second regime approximates the parameter Böttcher coordinate itself and is used for the exterior-geometry visualization containing numerical parameter rays.

8.1.1. Fixed-Index and First-Escape Approximations

For a parameter $c \in \mathbb{C}$, let $z_n(c)$ be the critical orbit polynomial defined by (52). Equivalently, (53) gives $z_n(c) = f_c^{\circ n}(0)$ .The finite critical orbit escape rate approximants introduced in Definition 3.6 are the quantities $G_n(c)$ defined in (30). By Corollary 5.4, the parameter Green function satisfies $G_{\mathcal{M}}(c) = 2g_c(0)$. Consequently, for a fixed index $N \geq 1$, define the fixed-index parameter Green-function approximation by

$$A_N(c) := 2G_N(c) = \frac{2}{2^N}\log^+|z_N(c)|. \tag{133}$$

The index N in (133) is fixed and is the same for every parameter c. This is the fixed-index approximation appearing in Theorem 8.1.

The grid-based numerical procedure used for visualization employs a different convention. Instead of evaluating every orbit at one common fixed index, it stops each orbit when that orbit first crosses a prescribed escape radius. The resulting quantity is therefore a variable-time estimator and must be distinguished from $A_N(c)$.

Let $N_{\max} \geq 1$ be a maximum iteration count and let $R_{\text{esc}} > 2$ be an escape radius. For a parameter c, define the truncated first-escape time by

$$\tau_{N_{\max}}(c) := \min\left\{1 \leq n \leq N_{\max} : |z_n(c)| > R_{\text{esc}}\right\}, \tag{134}$$

provided that the set in (134) is nonempty. If $\tau_{N_{\max}}(c)$ is defined, the variable-time first-escape estimator is

$$\hat{G}_{\text{esc}}(c) := 2G_{\tau_{N_{\max}}(c)}(c) = \frac{2}{2^{\tau_{N_{\max}}(c)}}\log\left|z_{\tau_{N_{\max}}(c)}(c)\right|. \tag{135}$$

The iteration index in (135) depends on c. Thus, the first-escape estimator is distinct from the fixed-index approximation (133). To apply Theorem 8.1 uniformly on a finite parameter grid $\mathcal{G}$, set $C_{\mathcal{G}} := \max_{c\in\mathcal{G}}|c|$ and choose $R_{\text{esc}} > \max\left\{2, \sqrt{2C_{\mathcal{G}}}\right\}$. Then, for every $c \in \mathcal{G}$, $R_{\text{esc}} > \max\left\{2, \sqrt{2|c|}\right\}$. If escape is detected at time $\tau_{N_{\max}}(c)$, then Theorem 8.1 applies with $n_0 = n = \tau_{N_{\max}}(c)$, and gives

$$\left|\hat{G}_{\text{esc}}(c) - G_{\mathcal{M}}(c)\right| \le \hat{E}_{\text{esc}}(c), \tag{136}$$

where

$$\hat{E}_{\text{esc}}(c) := \frac{2}{2^{\tau_{N_{\max}}(c)}}\left[-\log\left(1 - \frac{|c|}{R_{\text{esc}}^2}\right)\right]. \tag{137}$$

If the orbit does not cross R_{esc} by iteration $N_{\max}$, the finite computation does not prove that $c \in \mathcal{M}$. It shows only that escape was not detected within the prescribed iteration budget. We therefore define the unresolved set

$$\mathcal{U}_{N_{\max}} := \left\{c \in \mathcal{G} : \left|z_n(c)\right| \le R_{\text{esc}} \text{ for every } 1 \le n \le N_{\max}\right\}. \tag{138}$$

The set in (138) is a finite-time numerical mask and need not coincide with $\mathcal{G} \cap \mathcal{M}$.

Algorithm 1. Variable-Time First-Escape Estimation of $G_{\mathcal{M}}$

Input: Finite parameter grid $\mathcal{G} \subset \mathbb{C}$, maximum iteration count $N_{\max}$, and an admissible escape radius R_{esc}

Output: First-escape estimator $\widehat{G}_{\text{esc}}$, error certificate $\widehat{E}_{\text{esc}}$, escape-time map $\tau_{N_{\max}}$, and unresolved mask $\mathcal{U}_{N_{\max}}$

$\mathcal{U}_{N_{\max}} \leftarrow \varnothing$
for all $c \in \mathcal{G}$ **do**
  $z \leftarrow 0$
  escaped $\leftarrow$ false
  for $n = 1, \ldots, N_{\max}$ **do**
    $z \leftarrow z^2 + c$
    if $|z| > R_{\text{esc}}$ **then**
      $\tau_{N_{\max}}(c) \leftarrow n$
      $\widehat{G}_{\text{esc}}(c) \leftarrow \dfrac{2}{2^n} \log|z|$
      $\widehat{E}_{\text{esc}}(c) \leftarrow \dfrac{2}{2^n}\left[-\log\left(1 - \dfrac{|c|}{R_{\text{esc}}^2}\right)\right]$
      escaped $\leftarrow$ true
      break
    end if
  end for
  if escaped $=$ false **then**
    $\widehat{G}_{\text{esc}}(c) \leftarrow$ undefined
    $\widehat{E}_{\text{esc}}(c) \leftarrow$ undefined
    $\tau_{N_{\max}}(c) \leftarrow$ undefined
    $\mathcal{U}_{N_{\max}} \leftarrow \mathcal{U}_{N_{\max}} \cup \{c\}$
  end if
end for
return $\widehat{G}_{\text{esc}}$, $\widehat{E}_{\text{esc}}$, $\tau_{N_{\max}}$, and $\mathcal{U}_{N_{\max}}$

Algorithm 1 is a variable-time numerical procedure. It does not compute a single fixed-index field $A_N(c) = 2G_N(c)$ with one common value of N. For every parameter whose escape is detected, Algorithm 1 computes the first-escape estimator defined in (135) and the error field defined in (137). Proposition 8.6 proves the certificate (136) under the stated escape-radius condition. The zero-filled field $\tilde{G}_{\text{disp}}$ is used only for visualization. In particular, the dark region in the corresponding figures represents parameters for which escape was not detected within $N_{\max}$ iterations. It should not be interpreted as a rigorous numerical certification of membership in $\mathcal{M}$.

The preceding definitions and Theorem 8.1 give the following certified numerical consequence.

Proposition 8.6 (Error Certificate for the First-escape Estimator). Let $c \in \mathcal{G} \setminus \mathcal{U}_{N_{\max}}$, and let $\tau := \tau_{N_{\max}}(c)$. Then $\hat{G}_{\text{esc}}(c) = 2G_\tau(c)$. Moreover, the error certificate (136) holds.

Proof. Since $c \notin \mathcal{U}_{N_{\max}}$, Algorithm 1 detects escape at the finite index $\tau = \tau_{N_{\max}}(c)$. Therefore, $|z_\tau(c)| > R_{\text{esc}}$. By the admissibility condition on R_{esc}, $R_{\text{esc}} > \max\left\{2, \sqrt{2|c|}\right\}$. Hence the hypotheses of Theorem 8.1 hold with $n_0 = n = \tau$. By the definition used in Algorithm 1,

$$\hat{G}_{\text{esc}}(c) = \frac{2}{2^\tau}\log|z_\tau(c)|. \tag{139}$$

Since $|z_\tau(c)| > R_{\text{esc}} > 2$, one has $\log^+|z_\tau(c)| = \log|z_\tau(c)|$. Therefore, (139) and (30) give

$$\hat{G}_{\text{esc}}(c) = 2G_\tau(c). \tag{140}$$

Applying (108) at $n = \tau$ gives

$$\begin{aligned} \left|\hat{G}_{\text{esc}}(c) - G_{\mathcal{M}}(c)\right| &= \left|2G_\tau(c) - G_{\mathcal{M}}(c)\right| \\ &\le \frac{2}{2^\tau}\left[-\log\left(1 - \frac{|c|}{R_{\text{esc}}^2}\right)\right] \\ &= \hat{E}_{\text{esc}}(c). \end{aligned} \tag{141}$$

□

***Remark* 8.7 (Fixed-index versus variable-time approximation).** The fixed-index approximation (133) uses the same prescribed iteration index N for every parameter. By contrast, Algorithm 1 computes the variable-time estimator (135), whose stopping time depends on c. The two quantities agree only when $N = \tau_{N_{\max}}(c)$. Accordingly, the first-escape estimator must not be denoted by $G_{\mathcal{M}}^{(N)}(c)$, since such notation suggests a common fixed iteration index.

For visualization, it is convenient to assign a dark zero value to parameters in the unresolved set. We therefore define the display field

$$\tilde{G}_{\text{disp}}(c) := \begin{cases} \hat{G}_{\text{esc}}(c), & c \in \mathcal{G} \setminus \mathcal{U}_{N_{\max}}, \\ 0, & c \in \mathcal{U}_{N_{\max}}. \end{cases} \tag{142}$$

The value zero in (142) is a visualization convention only. It does not assert that every parameter in $\mathcal{U}_{N_{\max}}$ belongs to $\mathcal{M}$, nor that $G_{\mathcal{M}}(c) = 0$ has been certified for those parameters by the finite computation.

Figure 2 displays the zero-filled visualization of the variable-time estimator $\hat{G}_{\text{esc}}$. Its contours are numerical level curves of the estimator, not exact equipotentials of $G_{\mathcal{M}}$, and the unresolved mask does not certify membership in $\mathcal{M}$.

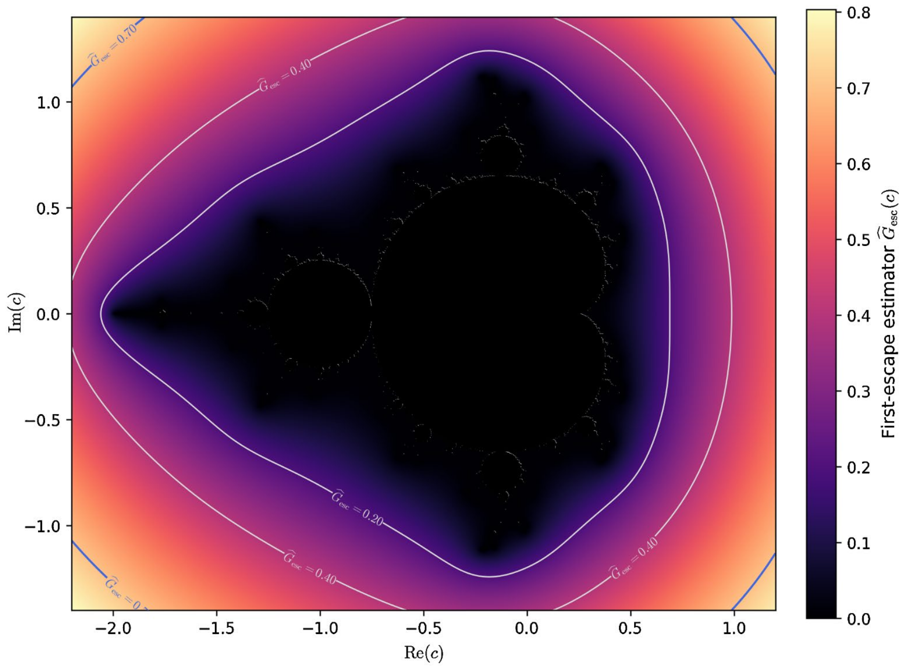

Figure 2. Variable-time first-escape approximation of the parameter Green function. The contours are level curves of $\hat{G}_{\text{esc}}(c)=2G_{\tau_{N_{\max}}(c)}(c)$. The black region is the finite-time unresolved mask, not a certified subset of $\mathcal{M}$. Proposition 8.6 provides the pointwise error bound.

8.1.2. Finite Dynamical-Plane Approximation

The dynamical-plane and parameter-plane computations use related but distinct normalizations. In the dynamical plane, the parameter c_0 is fixed and the initial point z_0 varies. In the parameter plane, the initial point is the critical point 0, while the parameter c varies. Figure 3 illustrates this distinction using the variable-time estimators $\hat{g}_{\text{esc}}$ and $\hat{G}_{\text{esc}}$.

For each initial point $z_0 \in \mathcal{Z}$, define the truncated dynamical first-escape time by

$$\tau_{N_{\max}}^{\text{dyn}}(z_0) := \min\left\{1 \le n \le N_{\max} : \left|f_{c_0}^{\circ n}(z_0)\right| > R_{\text{esc}}\right\}. \tag{143}$$

provided that the set on the right-hand side is nonempty. Whenever $\tau_{N_{\max}}^{\text{dyn}}(z_0)$ is defined, the dynamical-plane first-escape estimator is

$$\hat{g}_{\text{esc}}(z_0) = \frac{1}{2^{\tau_{N_{\max}}^{\text{dyn}}(z_0)}} \log\left|f_{c_0}^{\circ\tau_{N_{\max}}^{\text{dyn}}(z_0)}(z_0)\right|. \tag{144}$$

No factor 2 is applied in the dynamical plane.

Algorithm 2. Variable-Time Dynamical First-Escape Approximation

Input: Fixed parameter c_0, grid of initial points $\mathcal{Z} \subset \mathbb{C}$, maximum iteration count $N_{\max}$, and escape radius $R_{\text{esc}} > 2$

Output: Dynamical first-escape estimator $\widehat{g}_{\text{esc}}$, escape-time map $\tau_{N_{\max}}^{\text{dyn}}$, and unresolved dynamical mask $\mathcal{U}_{N_{\max}}^{\text{dyn}}$

$\mathcal{U}_{N_{\max}}^{\text{dyn}} \leftarrow \varnothing$
for all $z_0 \in \mathcal{Z}$ **do**
  $z \leftarrow z_0$
  escaped $\leftarrow$ false
  for $n = 1, \ldots, N_{\max}$ **do**
    $z \leftarrow z^2 + c_0$
    if $|z| > R_{\text{esc}}$ **then**
      $\tau_{N_{\max}}^{\text{dyn}}(z_0) \leftarrow n$
      $\widehat{g}_{\text{esc}}(z_0) \leftarrow \dfrac{1}{2^n} \log |z|$
      escaped $\leftarrow$ true
      break
    end if
  end for
  if escaped $=$ false **then**
    $\widehat{g}_{\text{esc}}(z_0) \leftarrow$ undefined
    $\tau_{N_{\max}}^{\text{dyn}}(z_0) \leftarrow$ undefined
    $\mathcal{U}_{N_{\max}}^{\text{dyn}} \leftarrow \mathcal{U}_{N_{\max}}^{\text{dyn}} \cup \{z_0\}$
  end if
end for
return $\widehat{g}_{\text{esc}}$, $\tau_{N_{\max}}^{\text{dyn}}$, and $\mathcal{U}_{N_{\max}}^{\text{dyn}}$

Algorithm 2 computes the variable-time dynamical first-escape estimator $\hat{g}_{\text{esc}}$ (144). Figure 3 compares the variable-time dynamical estimator $\hat{g}_{\text{esc}}$ for a fixed parameter c_0 with the parameter-plane display field $\tilde{G}_{\text{disp}}$. The two panels illustrate the different dynamical and parameter normalizations, rather than exact pointwise evaluations of g_{c_0} and $G_{\mathcal{M}}$.

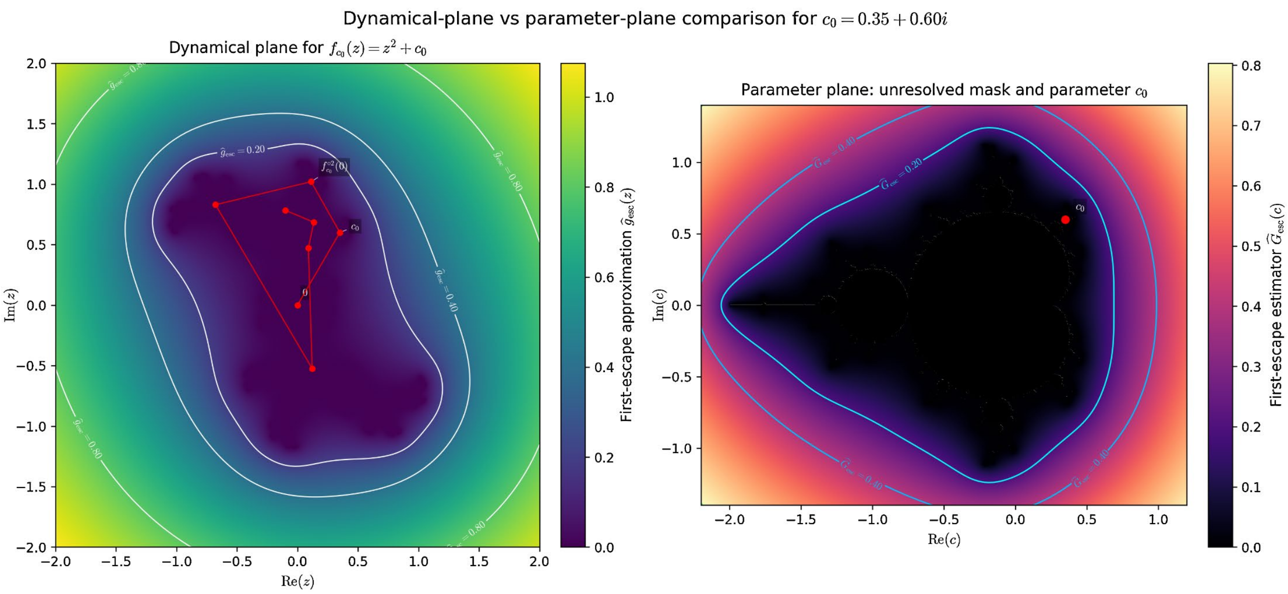

Figure 3. Dynamical-plane and parameter-plane first-escape visualizations for $f_c(z) = z^2 + c$. Left: the variable-time approximation $\hat{g}_{\text{esc}}(z)$ for a fixed escaping parameter c_0. Right: the zero-filled display field $\tilde{G}_{\text{disp}}$, constructed from $\hat{G}_{\text{esc}}(c) = 2G_{\tau_{N_{\max}}(c)}(c)$. The dark regions are finite-time unresolved masks and do not certify membership in the corresponding filled Julia set or in $\mathcal{M}$.

8.1.3. Numerical Approximation of the Parameter Böttcher Coordinate

The exterior-geometry visualization in Figure 4 requires more than the modulus of $\Phi_{\mathcal{M}}$. To draw parameter external rays, one also needs the argument of $\Phi_{\mathcal{M}}$. We therefore introduce the logarithmic coordinate

$$L(c) := \log \Phi_{\mathcal{M}}(c), \tag{145}$$

understood through compatible logarithmic branches on the exterior domain under consideration.

For $c \in \mathbb{C} \setminus \mathcal{M}$, the parameter Böttcher map is related to the dynamical exterior coordinate through the normalized pullback relation (78). The conventional notation $\Phi_{\mathcal{M}}(c) = \phi_c(c)$ is understood only in this normalized pullback sense, as explained in Theorem 4.8 and *Remark* 4.11. For the numerical construction, define the forward orbit of the critical value by

$$q_0(c) := c,\ \ q_{k+1}(c) := q_k(c)^2 + c,\ \ k \geq 0. \tag{146}$$

Since $q_0(c) = c = f_c(0)$, the orbit in (146) satisfies $q_k(c) = f_c^{\circ k}(c) = z_{k+1}(c)$. The recurrence (146) admits the factorization

$$q_{k+1}(c) = q_k(c)^2 \left(1 + \frac{c}{q_k(c)^2}\right). \tag{147}$$

On a parameter domain where compatible logarithmic branches have been selected, taking logarithms in (147) gives

$$\log q_{k+1}(c) = 2\log q_k(c) + \log\left(1 + \frac{c}{q_k(c)^2}\right). \tag{148}$$

Iterating (148) and selecting the branches compatibly with the normalization (36) yields the formal Böttcher-logarithm expansion

$$\log \Phi_{\mathcal{M}}(c) = \log c + \sum_{k=0}^{\infty} 2^{-(k+1)} \log\left(1 + \frac{c}{q_k(c)^2}\right). \tag{149}$$

The logarithms in (149) are understood through branches selected compatibly by analytic continuation from the normalization at infinity. Accordingly, (149) is used here as a local branch-compatible representation rather than as an independent branch-free global definition of $\Phi_{\mathcal{M}}$. For a truncation depth $K \geq 1$, define

$$L_K(c) := \log c + \sum_{k=0}^{K-1} 2^{-(k+1)} \log\left(1 + \frac{c}{q_k(c)^2}\right). \tag{150}$$

The real part of the truncated logarithmic coordinate defines the numerical potential field

$$G_{\mathcal{M}}^{(K)}(c) := \operatorname{Re} L_K(c). \tag{151}$$

Since $\operatorname{Re}\log \Phi_{\mathcal{M}}(c) = \log\left|\Phi_{\mathcal{M}}(c)\right|$, the field in (151) is intended to approximate the exact parameter Green function $G_{\mathcal{M}}(c)$ defined in (82). It is used to produce the numerical potential background and the approximate equipotential curves in **Figure 4**. The imaginary part of the truncated logarithmic coordinate defines the numerical external-angle field

$$\Theta_K(c) := \frac{\operatorname{Im} L_K(c)}{2\pi} \pmod 1. \tag{152}$$

The division by 2π expresses the argument in turns, consistently with the angular convention in Definition 7.1. Thus, (152) is intended to approximate the external argument $\arg \Phi_{\mathcal{M}}(c)/(2\pi) \pmod 1$. The field is used in the numerical extraction of parameter-ray segments described in Algorithm 4. Because the computation depends on compatible logarithmic branches, no global branch-certified error estimate for Θ_K is asserted. Taken together, the numerical potential and external-angle fields defined in (151) and (152), respectively, are obtained from the real and imaginary parts of the truncated logarithmic coordinate (150).

Algorithm 3. Truncated Böttcher-Logarithm Approximation

Input: Exterior parameter c, truncation depth K, overflow threshold R_{overflow}

Output: Approximate logarithmic coordinate $L_K(c)$, potential $G_{\mathcal{M}}^{(K)}(c)$, angle $\Theta_K(c)$

```
q ← c
L ← log c
for k = 0, ..., K − 1 do
    if q is nonfinite or |q| ≥ R_overflow then
        break
    end if
    L ← L + 2^(−(k+1)) log(1 + c/q^2)
    q ← q^2 + c
end for
L_K(c) ← L
G_M^(K)(c) ← max{Re L_K(c), 0}
Θ_K(c) ← Im L_K(c)/(2π) (mod 1)
return L_K(c), G_M^(K)(c), and Θ_K(c)
```

In the numerical implementation of Algorithm 3, small negative values of $\operatorname{Re} L_K(c)$ are replaced by zero through the assignment $\max\{\operatorname{Re} L_K(c), 0\}$. This clipping is an implementation safeguard, used to suppress small negative values caused by truncation and floating-point roundoff. It is an implementation and visualization convention and is not part of the mathematical definition (151). Algorithm 3 is used in **Figure 4**. The white curves are level curves of $G_{\mathcal{M}}^{(K)}$, while the coloured curves are extracted from the numerical angle field Θ_K. These provide finite-resolution approximations to the exact equipotentials and parameter external rays of Definition 7.1; they are not identified with the exact conformal objects.

8.1.4. Numerical Extraction of Parameter External Rays

For an external angle $\theta \in \mathbb{R}/\mathbb{Z}$, the exact parameter external ray is defined by Definition 7.1 and (106). Numerically, Θ is replaced by Θ_K. Direct contouring of $\Theta_K = \theta$ is inconvenient because Θ_K is defined modulo 1. To remove this discontinuity, define

$$F_\theta(c) := \sin\left(2\pi\left(\Theta_K(c) - \theta\right)\right). \tag{153}$$

The equation $F_\theta(c) = 0$ contains both $\Theta_K(c) = \theta(\operatorname{mod} 1)$ and $\Theta_K(c) = \theta + \frac{1}{2}(\operatorname{mod} 1)$. The desired branch is selected by imposing

$$\cos\left(2\pi\left(\Theta_K(c) - \theta\right)\right) > 0. \tag{154}$$

In addition, the computation is restricted to points satisfying $G_{\mathcal{M}}^{(K)}(c) > \varepsilon_G$, where $\varepsilon_G > 0$ is a small numerical cutoff. This avoids extracting rays from points too close to the unresolved boundary level $G_{\mathcal{M}} = 0$. Condition (154) selects the branch corresponding to angle θ.

Algorithm 4. Extraction of a Numerical Parameter External Ray

---

Input: External angle θ, fields Θ_K and $G_{\mathcal{M}}^{(K)}$, finite-time valid-domain mask, cutoff ε_G, and plotting window D

Output: Principal numerical ray segment $\mathcal{R}_\theta^{(K)}$

for all valid grid points c **do**
  $\Delta_\theta(c) \leftarrow \Theta_K(c) - \theta$
  $F_\theta(c) \leftarrow \sin(2\pi\Delta_\theta(c))$
  $B_\theta(c) \leftarrow (\cos(2\pi\Delta_\theta(c)) > 0)$
  $\mathrm{valid}(c) \leftarrow B_\theta(c)$ and $G_{\mathcal{M}}^{(K)}(c) > \varepsilon_G$
end for
Mask F_θ outside the valid region
Extract all zero-contour components of $F_\theta(c) = 0$
Discard components with too few points
Prefer components intersecting the boundary of D
Select the admissible component with maximal Euclidean arc length
Orient the selected component from the exterior frame toward $\mathcal{M}$
return the selected component as $\mathcal{R}_\theta^{(K)}$

The component-selection rule in Algorithm 4 is a numerical post-processing step. It is not part of the theoretical definition of $\mathcal{R}_\theta$. The theoretical definition remains the conformal one given in Definition 7.1.

8.1.5. Display Field and Contrast Enhancement

The colour background in Figure 4 does not display the raw Green function directly. Instead, for visual contrast, it uses the monotone transformation

$$\tilde{G}_{\mathcal{M}}^{(K)}(c) := \log\left(1 + \alpha G_{\mathcal{M}}^{(K)}(c)\right), \quad \alpha > 0. \tag{155}$$

The transformed field defined in (155) is used only to enhance visual contrast.

The white curves in **Figure 4** are level curves of the untransformed numerical potential $G_{\mathcal{M}}^{(K)}$, while the exact equipotentials are defined in (105). Thus, the figure is a finite-resolution illustration of the exact conformal identity established in Proposition 7.2 and (107), rather than an exact numerical reconstruction of the exterior geometry. Since $x \mapsto \log(1+\alpha x)$ is strictly increasing for $x \geq 0$, this transformation preserves the order of potential values. It is used only to improve the visibility of small potential variations near $\partial\mathcal{M}$. The actual equipotential curves in **Figure 4** are contours of the untransformed quantity $G_{\mathcal{M}}^{(K)}$, not contours of the colourbar variable. The finite-time unresolved region is displayed in a dark indigo colour. This is a visualization convention only. Analytically, the exact zero-potential set is $\mathcal{M}$, but the finite-time unresolved mask need not coincide exactly with $\mathcal{M}$. No exterior Green-function value is certified for parameters in the unresolved mask.

8.1.6. Complete Exterior-Geometry Visualization

The final exterior-geometry visualization combines four numerical objects: the finite-time unresolved mask, the transformed display field $\tilde{G}_{\mathcal{M}}^{(K)}$, the level curves of $G_{\mathcal{M}}^{(K)}$, and the numerical parameter external rays extracted from Θ_K.

Algorithm 5. Complete Finite-Resolution Exterior-Geometry Visualization

Input: Finite-time unresolved mask, $G_{\mathcal{M}}^{(K)}$, Θ_K, $\tilde{G}_{\mathcal{M}}^{(K)}$, contour levels, and selected external angles
Output: Exterior-geometry visualization

```
Plot G̃_M^(K) as the coloured exterior background
Draw level curves G_M^(K)(c) = t
Label only a sparse subset of the numerical level curves
for all selected external angles θ do
    Apply Algorithm 4 to obtain R_θ^(K)
    Plot R_θ^(K) using its assigned colour
    Place the angle label near a stable point of the ray
end for
Fill the finite-time unresolved region using a dark low-energy colour
Add a subdued boundary highlight, axis labels, and colourbar
Save the figure in raster and vector formats
```

Algorithm 5 supports **Figure 4**. The figure should be read as a finite-resolution numerical illustration of the exact equipotential identity established in Proposition 7.2 and (107), together with the exact parameter-ray definition in Definition 7.1 and (106).

The display transformation affects only the visual contrast and does not alter the numerical level curves used in the figure. All equipotential and ray components shown in **Figure 4** should therefore be interpreted as finite-resolution numerical approximations.

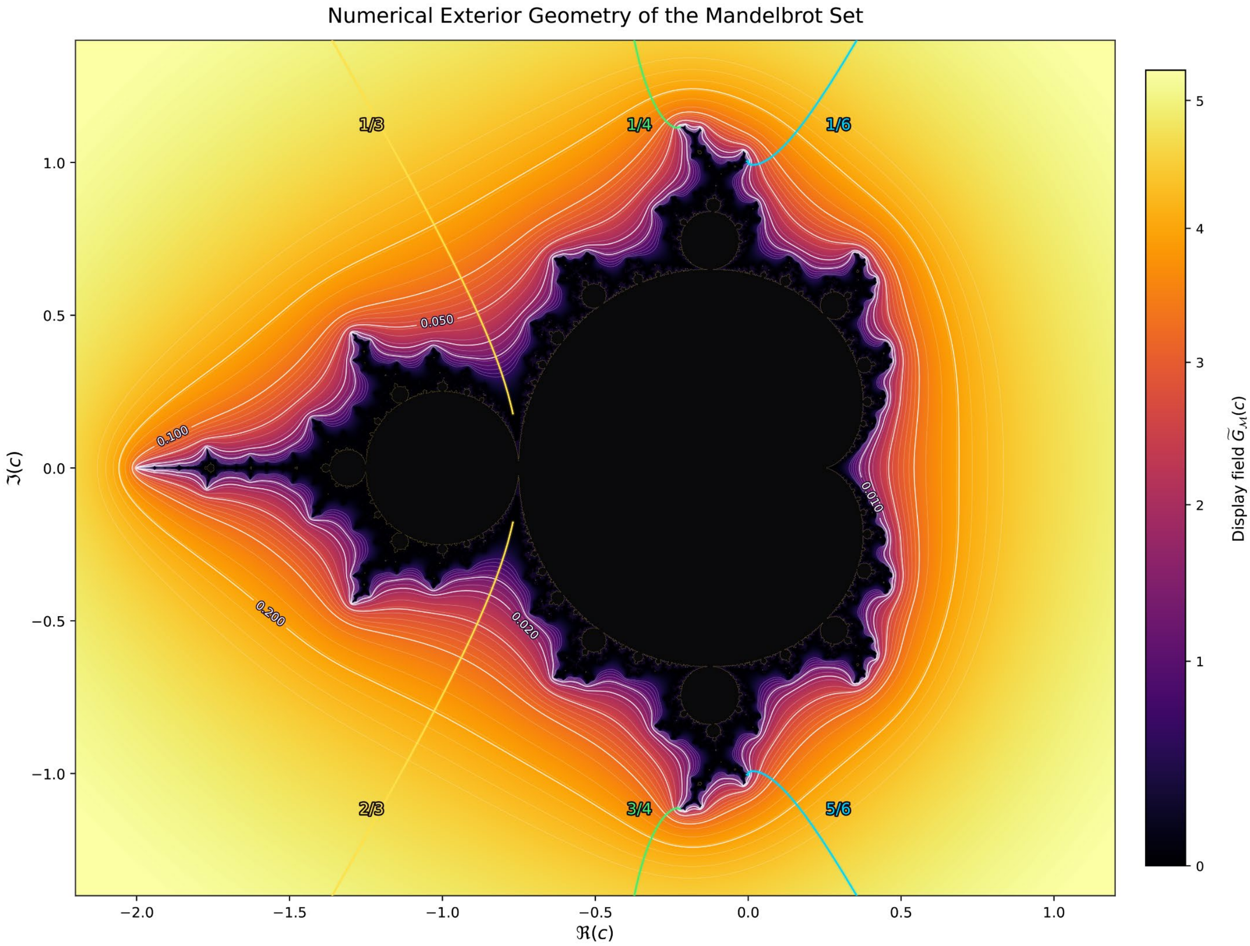

Figure 4. Numerical exterior geometry obtained from a truncated Böttcher coordinate. The transformed background $\tilde{G}_{\mathcal{M}}^{(K)}$ is used for visual contrast, the white curves are level curves of $G_{\mathcal{M}}^{(K)}$, and the coloured curves approximate parameter external rays. The computation uses a 1700 × 1300 grid, $N_{\max} = 650$, $R_{\text{esc}} = 200$, $K = 30$, and $\alpha = 220$. The dark region is the finite-time unresolved mask.

8.1.7. Numerical Convergence and Certified Comparison Bounds

For representative escaping parameters, we consider the fixed-index approximants $A_n(c)$ defined in (133). For each such parameter, the numerical reference value $G_{\text{ref}}(c)$ is computed by a variable-time first-escape calculation using a sufficiently large admissible reference radius R_{ref}. The associated error certificate satisfies

$$\left|G_{\text{ref}}(c) - G_{\mathcal{M}}(c)\right| \le E_{\text{ref}}(c). \tag{156}$$

Thus, the certificate (156) controls the discrepancy between the numerical reference value and the exact Green function. For an admissible theorem radius R, define

$$B_n(c;R) := \frac{2}{2^n}\left[-\log\left(1 - \frac{|c|}{R^2}\right)\right]. \tag{157}$$

Suppose that the critical orbit has entered the corresponding escape region by an index n_0. Then Theorem 8.1, together with the error estimate (108), the fixed-index definition (133), and the conformal identity (82), gives, for every $n \geq n_0$,

$$\left|A_n(c) - G_{\mathcal{M}}(c)\right| \leq B_n(c;R). \tag{158}$$

Combining the fixed-index error bound (158) with the numerical-reference certificate (156), the triangle inequality gives

$$\begin{aligned}\left|A_n(c) - G_{\mathrm{ref}}(c)\right| &\leq \left|A_n(c) - G_{\mathcal{M}}(c)\right| + \left|G_{\mathcal{M}}(c) - G_{\mathrm{ref}}(c)\right| \\ &\leq B_n(c;R) + E_{\mathrm{ref}}(c), \quad n \geq n_0.\end{aligned} \tag{159}$$

For convenience, define the plotted certified comparison bound by

$$C_n(c;R) := B_n(c;R) + E_{\mathrm{ref}}(c). \tag{160}$$

With the notation (160), the comparison estimate (159) becomes $\left|A_n(c) - G_{\mathrm{ref}}(c)\right| \leq C_n(c;R)$ for every $n \geq n_0$.

Algorithm 6. Fixed-Index Convergence and Certified Comparison Bounds

Input: Escaping parameters $\{c_j\}_{j=1}^{m}$, iteration limit N, theorem radius R, reference radius R_{ref}

Output: Fixed-index sequences, numerical-reference discrepancies, and certified comparison bounds

for all $c_j \in \{c_1, \dots, c_m\}$ **do**
  Compute $A_n(c_j) = 2G_n(c_j)$ for $n = 1, \dots, N$
  Compute the first-escape reference $G_{\mathrm{ref}}(c_j)$ using R_{ref}
  Compute the corresponding error certificate $E_{\mathrm{ref}}(c_j)$
  Determine the first index $n_0(c_j)$ satisfying $|z_{n_0(c_j)}(c_j)| \geq R$
  for $n = n_0(c_j), \dots, N$ **do**
    Set $B_n(c_j;R) \leftarrow \frac{2}{2^n}\left[-\log\left(1 - \frac{|c_j|}{R^2}\right)\right]$
    Set $C_n(c_j;R) \leftarrow B_n(c_j;R) + E_{\mathrm{ref}}(c_j)$
  end for
  Plot $A_n(c_j)$ and $G_{\mathrm{ref}}(c_j)$
  Plot $|A_n(c_j) - G_{\mathrm{ref}}(c_j)|$ and $C_n(c_j;R)$ on a logarithmic scale
end for
return the convergence and certified-bound plots

Algorithm 6 produces the numerical visualization shown in **Figure 5**. Its mathematical justification is provided by Theorem 8.1 and the fixed-index error estimate (158). The figure illustrates the convergence of the fixed-index approximants $A_n(c)$, defined in (133), for representative escaping parameters. The displayed discrepancies are computed relative to the certified numerical reference $G_{\mathrm{ref}}(c)$, whose error is controlled by (156). The dotted curves represent the plotted certified comparison bound $C_n(c;R)$ defined in (160). By (159), these curves provide upper **bounds** for the discrepancies $\left|A_n(c) - G_{\mathrm{ref}}(c)\right|$ at every index $n \geq n_0$ for which the corresponding critical orbit has entered the prescribed escape region. The semilogarithmic decay shown in **Figure 5** is consistent with the exponential estimate (108) proved in Theorem 8.1. The figure is a finite-resolution numerical illustration and is not used to establish the convergence or the certified bounds.

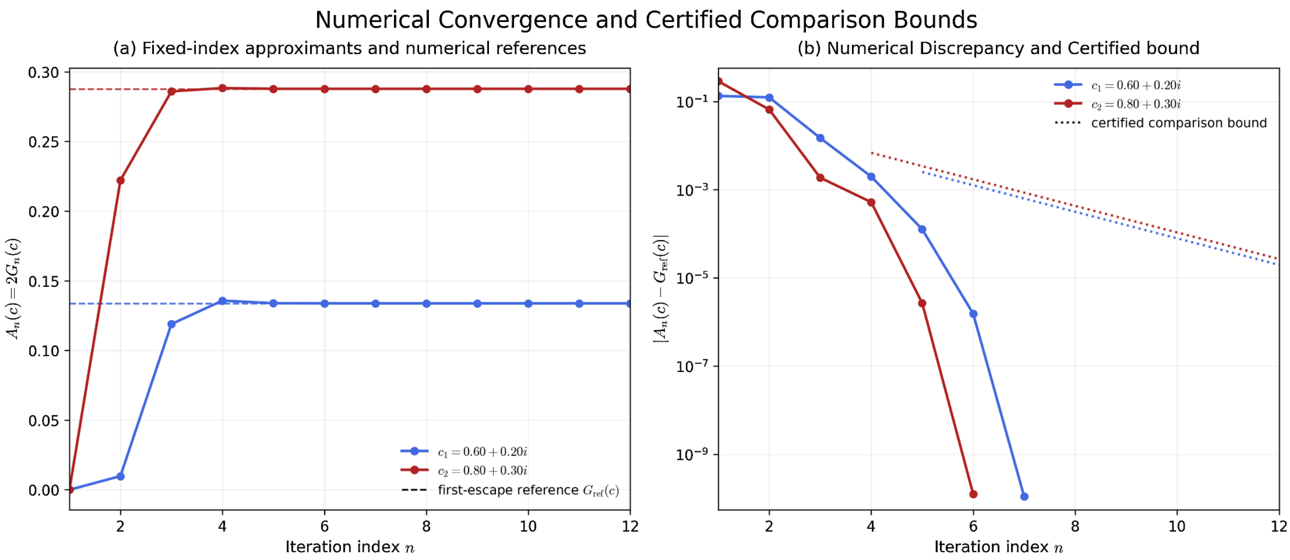

Figure 5. Convergence of the fixed-index approximants $A_n(c)$, defined in (133), for two representative escaping parameters. The dashed lines are the first-escape references $G_{\mathrm{ref}}(c)$, computed using $R_{\mathrm{ref}} = 10^6$. The right panel compares the discrepancies $|A_n(c) - G_{\mathrm{ref}}(c)|$ with the certified bounds $C_n(c;4)$ defined by (160), with the admissible theorem radius $R = 4$.

8.1.8. First-Escape Level-Curve Visualization

Figure 6 is generated from the variable-time first-escape estimator $\hat{G}_{\mathrm{esc}}$ defined in (135) and computed by Algorithm 1. The highlighted curves are numerical level curves of $\hat{G}_{\mathrm{esc}}$ at the levels $t-\delta$, t, and $t+\delta$, with $t = 0.160$ and $\delta = 0.024$. Thus, the displayed numerical levels are 0.136, 0.160, and 0.184. These curves provide a finite-resolution illustration of the Hausdorff-continuity result proved later in Theorem 9.1. They are numerical level curves of the estimator $\hat{G}_{\mathrm{esc}}$, not the exact equipotentials E_t defined in (105). Furthermore, the unresolved region is the finite-time mask defined in (138) and does not certify membership in $\mathcal{M}$.

Algorithm 7. Nearby Level Curves of the First-Escape Estimator

Input: First-escape estimator $\widehat{G}_{\mathrm{esc}}$, unresolved mask $\mathcal{U}_{N_{\max}}$, level $t > 0$, and perturbation $0 < \delta < t$

Output: Three nearby numerical level curves

1: Define the levels $t-\delta$, t, and $t+\delta$
2: Plot a background field for $\widehat{G}_{\mathrm{esc}}$ outside $\mathcal{U}_{N_{\max}}$
3: Extract the level curves $\widehat{G}_{\mathrm{esc}}(c) = t-\delta$, $\widehat{G}_{\mathrm{esc}}(c) = t$, $\widehat{G}_{\mathrm{esc}}(c) = t+\delta$
4: Highlight the central level $\widehat{G}_{\mathrm{esc}}(c) = t$
5: Display the three curves using distinct colours
6: Fill $\mathcal{U}_{N_{\max}}$ using the unresolved-mask colour
7: **return** the nearby-level-curve visualization

Algorithm 7 generates the numerical level curves shown in Figure 6. The figure is a finite-resolution illustration of Theorem 9.1; it is not used in the *proof.*

8.1.9. Schematic Uniformization Figure

Figure 1 is schematic rather than a direct numerical inversion of the parameter

Böttcher map. It illustrates the conformal correspondence supplied by Theorem 4.8. Under this correspondence, the exact equipotentials are the inverse images of the circles C_t, as established in Proposition 7.2 and (107), while the exact parameter external rays are defined by Definition 7.1 and (106). The schematic parameter external ray is included only to explain the geometry of the uniformization and is not presented as a numerically computed inverse Böttcher ray. The computed numerical ray segments appear instead in **Figure 4**, where they are extracted from the external-angle field Θ_K defined in (152), itself obtained from the truncated logarithmic coordinate (150).

8.1.10. Implementation and Numerical Limitations

The numerical methods use array-based complex iteration on finite grids and standard contour extraction for scalar fields. The computations were implemented using NumPy for array operations and Matplotlib for plotting and contour visualization; see [21] [22]. Several safeguards are used in the implementation:

(i) The Böttcher-logarithm computation is restricted to parameters for which exterior escape has been detected by the finite escape test;

(ii) Orbit updates are stopped before floating-point overflow;

(iii) Non–finite values are rejected;

(iv) In the implementation of Algorithm 3, small negative values of $\operatorname{Re} L_K(c)$, caused by truncation or floating-point roundoff, are replaced by 0, as explained after (151);

(v) Ray extraction is restricted to points satisfying $G_{\mathcal{M}}^{(K)}(c) > \varepsilon_G$, where $G_{\mathcal{M}}^{(K)}$ is defined in (151); this restriction avoids the numerically unresolved boundary region;

(vi) Among admissible ray components, preference is given to components reaching the plotting boundary.

Near $\partial\mathcal{M}$, both escape detection and Böttcher-coordinate approximation converge more slowly. Consequently, all plotted equipotentials and rays near the boundary should be interpreted as finite-resolution numerical approximations.

***Remark* 8.8.** The truncated Böttcher-logarithm approximation $L_K(c)$, defined in (150), is introduced only for numerical visualization of equipotentials and parameter external rays. It is not used as an additional hypothesis in any of the analytic proofs of the paper.

***Remark* 8.9.** All numerical figures in this paper are finite-resolution visualizations of the analytic theory. The exact conformal construction is Definition 5.1, the exact parameter-space uniformization is Theorem 4.8, the exact equipotential identity is Proposition 7.2, and the convergence mechanism for finite critical orbit approximants is Theorem 8.1. The numerical plots are therefore illustrations of these results, not additional hypotheses or substitutes for the proofs.

9. Stability of Equipotentials Away from the Boundary

We now strengthen the geometric interpretation of the level sets of $G_{\mathcal{M}}$ by proving a stability statement for equipotentials lying a positive distance away from the boundary of the Mandelbrot set.

Theorem 9.1 (**Hausdorff Continuity of Equipotentials on Compact Level Ranges**). *Let* $0<a<b$. *For each* $t\in[a,b]$, *let* E_t *be the equipotential defined in Definition 7.1 and (105). Then the family* $\{E_t\}_{t\in[a,b]}$ *depends continuously on* t *in the Hausdorff topology of Definition 3.12. More precisely, if* $t_n\to t$ *in* $[a,b]$, *then*

$$d_{\mathrm{H}}\left(E_{t_n},E_t\right)\to 0. \tag{161}$$

Proof. By Proposition 7.2 and (107), $E_t=\Phi_{\mathcal{M}}^{-1}\left(C_t\right)$, where C_t is the exterior circle defined in Notation 3.13 and (38). Since $C_t\subset\mathbb{C}\setminus\overline{\mathbb{D}}$ is nonempty and compact and $\Phi_{\mathcal{M}}^{-1}$ is continuous on $\mathbb{C}\setminus\overline{\mathbb{D}}$, the equipotential $E_t=\Phi_{\mathcal{M}}^{-1}\left(C_t\right)$ is nonempty and compact.

Let $A_{a,b}$ be the compact annulus introduced in Notation 3.13. Since $0<a<b$, one has $A_{a,b}\subset\mathbb{C}\setminus\overline{\mathbb{D}}$. By Theorem 4.8, the inverse map $\Phi_{\mathcal{M}}^{-1}$ is continuous on $\mathbb{C}\setminus\overline{\mathbb{D}}$, and hence is uniformly continuous on the compact set $A_{a,b}$. If $t_n\to t$, then C_{t_n} and C_t lie in $A_{a,b}$. Moreover, their Hausdorff distance is

$$d_{\mathrm{H}}\left(C_{t_n},C_t\right)=\left|\mathrm{e}^{t_n}-\mathrm{e}^{t}\right|\to 0. \tag{162}$$

Let $\omega_{a,b}$ be a modulus of uniform continuity for $\Phi_{\mathcal{M}}^{-1}$ on $A_{a,b}$. Then

$$d_{\mathrm{H}}\left(\Phi_{\mathcal{M}}^{-1}\left(C_{t_n}\right),\Phi_{\mathcal{M}}^{-1}\left(C_t\right)\right)\le\omega_{a,b}\left(d_{\mathrm{H}}\left(C_{t_n},C_t\right)\right)\to 0. \tag{163}$$

Using Proposition 7.2 again, (163) gives (161). □

***Remark* 9.2.** For $0<a<b$, define the positive-potential band

$$\Omega_{a,b}:=\left\{c\in\mathbb{C}\setminus\mathcal{M}:a\le G_{\mathcal{M}}\left(c\right)\le b\right\}. \tag{164}$$

By the conformal representation (82) and the definition of the compact annulus $A_{a,b}$ in Notation 3.13, one has

$$\Omega_{a,b}=\Phi_{\mathcal{M}}^{-1}\left(A_{a,b}\right). \tag{165}$$

Since $A_{a,b}$ is compact and $\Phi_{\mathcal{M}}^{-1}$ is continuous, (165) shows that $\Omega_{a,b}$ is compact. Consequently, Corollary 8.4 gives constants $n_{a,b}\ge 1$ and $C_{a,b}>0$ such that

$$\sup_{c\in\Omega_{a,b}}\left|2G_n\left(c\right)-G_{\mathcal{M}}\left(c\right)\right|\le C_{a,b}2^{-n},\ \ n\ge n_{a,b}. \tag{166}$$

Thus, the fixed-index approximants converge uniformly and exponentially on every compact positive-potential band.

Figure 6 displays three nearby positive level curves of the variable-time first-escape estimator $\hat{G}_{\mathrm{esc}}$, defined in (135). These curves are finite-resolution numerical illustrations and are not identified with the exact equipotentials E_t defined in (105). The displayed levels lie in a compact subinterval of $(0,\infty)$, so their ordered variation is consistent with Theorem 9.1 and the exact conformal description established in Proposition 7.2 and (107). The figure is not used in the proof of Hausdorff continuity. Combining Theorem 9.1 with the exact pullback identity gives the following structural consequence.

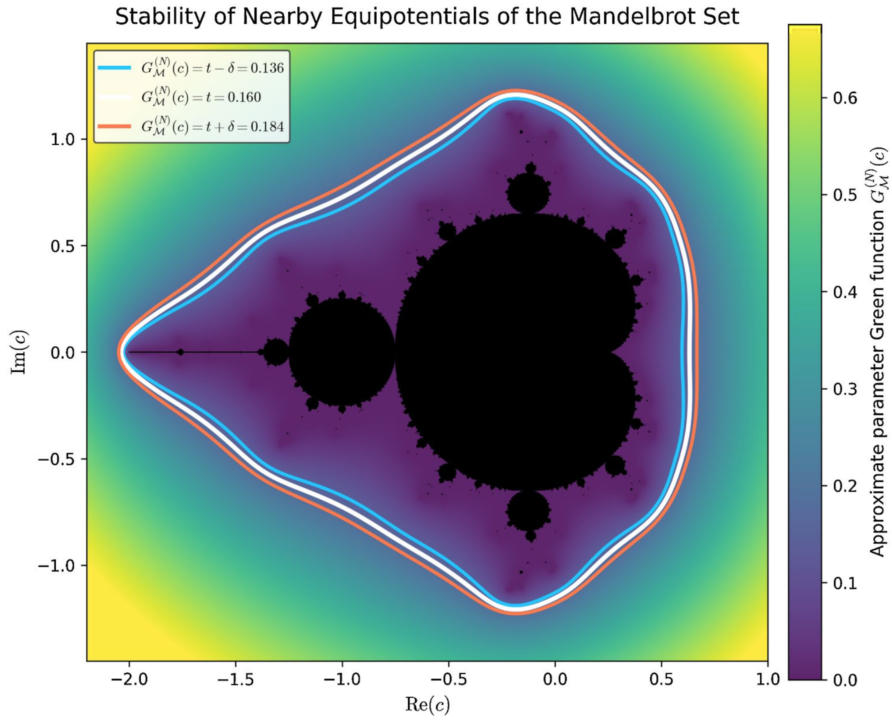

Figure 6. Finite-resolution level curves of the first-escape estimator $\hat{G}_{\text{esc}}$, defined in (135), computed with $N_{\max}=650$ and $R_{\text{esc}}=200$ at the levels 0.136, 0.160, and 0.184. The dark region is the finite-time unresolved mask defined in (138). The curves provide a finite-resolution illustration consistent with the Hausdorff continuity established in Theorem 9.1.

Corollary 9.3 (Continuous Family of Compact Equipotentials). *For every compact interval* $[a,b]\subset(0,\infty)$, *the equipotentials* $\{E_t\}_{t\in[a,b]}$ *form a pairwise disjoint, Hausdorff-continuous family of compact sets whose union is the positive-potential band* $\Omega_{a,b}$ *defined in* (164).

Proof. By Definition 7.1 and (105), E_t is the level set of $G_{\mathcal{M}}$ at height t. Let $c\in\Omega_{a,b}$. By (164), $a\le G_{\mathcal{M}}(c)\le b$. Setting $t:=G_{\mathcal{M}}(c)$, one has $t\in[a,b]$ and $c\in E_t$. Therefore, $\Omega_{a,b}\subseteq\sum_{t\in[a,b]}E_t$.

Conversely, if $c\in E_t$ for some $t\in[a,b]$, then $G_{\mathcal{M}}(c)=t\in[a,b]$, and hence $c\in\Omega_{a,b}$. Consequently,

$$\Omega_{a,b}=\bigcup_{t\in[a,b]}E_t. \tag{167}$$

The equipotentials are pairwise disjoint. Indeed, if $c\in E_s\cap E_t$, then $G_{\mathcal{M}}(c)=s$ and $G_{\mathcal{M}}(c)=t$, so $s=t$. Thus, every point of $\Omega_{a,b}$ lies on exactly one equipotential. By Proposition 7.2 and (107), one has $E_t=\Phi^{-1}_{\mathcal{M}}(C_t)$. Since C_t is compact and $\Phi^{-1}_{\mathcal{M}}$ is continuous on $\mathbb{C}\setminus\overline{\mathbb{D}}$, each E_t is compact. Finally, Theorem 9.1 and (161) show that $t\mapsto E_t$ is continuous on $[a,b]$ in the Hausdorff topology of Definition 3.12. Therefore, $\{E_t\}_{t\in[a,b]}$ forms a pairwise disjoint, Hausdorff-continuous family of compact equipotentials covering $\Omega_{a,b}$.

□

***Remark* 9.4.** Theorem 9.1 makes precise the geometric idea that, away from the boundary $\partial\mathcal{M}$, the equipotentials of the Mandelbrot set vary in a controlled and conformally natural manner. This strengthens the descriptive role of Section 7 by replacing interpretation with a theorem on the geometry of level sets.

10. Relation with Quantitative Escape-Rate Theory

We now make explicit the relation between the present paper and [6]. This section records the conceptual consequence of Corollary 5.4 and Theorem 8.1 in the notation of the earlier quantitative paper.

Proposition 10.1. *For* $c \in \mathbb{C}\setminus\mathcal{M}$, *let* $\mathcal{G}(c) := g_c(0)$. *Then* $G_{\mathcal{M}}(c) = 2\mathcal{G}(c)$. *Let* $\mathcal{G}_n(c)$ *denote the finite critical orbit approximant used in* [6], t*hen, under the identification* $\mathcal{G}_n(c) = G_n(c)$ *with the notation of Definition* 3.6, *one has*

$$2\mathcal{G}_n(c) \to G_{\mathcal{M}}(c) \ (n \to \infty). \tag{168}$$

Proof. The identity $G_{\mathcal{M}}(c) = 2\mathcal{G}(c)$ is Corollary 5.4. Moreover, by Definition 3.5 and (31), $\mathcal{G}_n(c) = G_n(c) \to g_c(0) = \mathcal{G}(c)$. Multiplying this convergence by 2 and using Corollary 5.4 gives (168). □

***Remark* 10.2.** Proposition 10.1 should not be read as a repetition of the quantitative theory of [6]. Rather, it provides the conceptual translation between the two frameworks. The earlier paper studies the convergence and effective computation of the critical-point escape-rate $\mathcal{G}(c)$, whereas the present one identifies the structurally natural parameter-plane Green function $G_{\mathcal{M}}(c)$ and characterizes it by conformal and potential-theoretic means.

***Remark* 10.3.** From the viewpoint of mathematical exposition, the two papers play complementary roles. The quantitative paper answers the question: how can one approximate the regularized escape-rate effectively and with error control? The present paper answers the different question: what is the precise analytic and geometric object being approximated? The answer is the unique Green function of $\mathbb{C}\setminus\mathcal{M}$ with pole at infinity, represented by the conformal identity (82).

11. Limitations of the Present Study

The results of this paper establish a quantitative connection between finite critical orbit escape rates and the classical exterior Green function of the Mandelbrot set. The following limitations identify questions that remain outside the scope of the present analysis.

(i) The theoretical analysis is restricted to the quadratic family $f_c(z) = z^2 + c$, introduced in Definition 3.1. No corresponding quantitative–conformal estimate is derived here for higher-degree unicritical polynomials, multiparameter polynomial families, rational maps, or transcendental maps.

(ii) The conformal construction of the parameter Green function in Definition 5.1 and (82) describes only the exterior domain $\mathbb{C}\setminus\mathcal{M}$. The present paper does not investigate the internal geometry of hyperbolic components, multiplier coordinates, parabolic bifurcations, or renormalization phenomena inside $\mathcal{M}$.

(iii) The quantitative estimate in Theorem 8.1 and (108) applies only after the critical orbit has entered a prescribed admissible escape region. It does not provide a parameter-dependent complexity estimate for the corresponding entry time, particularly as c approaches $\partial\mathcal{M}$.

(iv) The unresolved set $\mathcal{U}_{N_{\max}}$, defined in (138) and computed by Algorithm 1, records only that escape was not detected within $N_{\max}$ iterations. Membership in $\mathcal{U}_{N_{\max}}$ does not certify membership in $\mathcal{M}$.

(v) The pointwise certificate $\hat{E}_{\text{esc}}(c)$, defined in (137), controls the potential-value error through (136). This scalar certificate does not, by itself, provide a certified Hausdorff bound for level curves extracted from a finite parameter grid.

(vi) The truncated Böttcher-logarithm approximation $L_K(c)$, defined in (150), is used only for numerical visualization. No global branch-certified error estimate is proved for the numerical external-angle field $\Theta_K(c)$ defined in (152). Consequently, no convergence theorem or certified geometric error bound is established for the numerical external-ray components extracted by Algorithm 4.

(vii) The equipotential-stability result in Theorem 9.1 applies only to compact positive level ranges $0 < a \le t \le b$. Equivalently, the theorem concerns equipotentials contained in the compact positive-potential bands defined in (164). The present manuscript does not establish an analogous uniform Hausdorff-stability result as $t \downarrow 0$, where the equipotentials approach the boundary regime associated with $\partial\mathcal{M}$.

(viii) The numerical figures depend on finite grid resolution, escape radii, iteration budgets, truncation depths, contour-interpolation and component-selection rules, and floating-point arithmetic. They are finite-resolution illustrations of the analytic theory and are not computer-assisted proofs of boundary membership, parameter-ray landing, or local connectivity.

These limitations do not affect the analytic results proved in the paper. Rather, they identify the points at which additional theoretical estimates, branch control, geometric stability arguments, or computer-assisted methods would be required.

12. Proposed Future Research Directions

The present results suggest a future programme centred on the conversion of pointwise escape-rate certificates into certified geometric information. The main objective is to pass from the certified scalar approximation supplied by Proposition 8.6 and (136) to certified approximations of the exact equipotentials and parameter external rays introduced in Definition 7.1. The statements below are proposed research targets. Except where a proof is supplied, they are not asserted as results of the present paper.

12.1. Primary Research Problem

Problem 12.1 (Certified Reconstruction of Exterior Geometry). Develop a finite algorithm that, for prescribed numbers $0 < a < b$ and $\varepsilon > 0$, produces numerical approximations to the exact equipotentials E_t, defined in (105), for every $t \in [a,b]$, together with a computable certificate guaranteeing that the Hausdorff error, measured using Definition 3.12, is at most ε. The certificate should depend explicitly on:

(a) The first-escape error field $\hat{E}_{\text{esc}}$ defined in (137);

(b) The parameter-grid mesh size;

(c) A lower bound for $|\nabla G_{\mathcal{M}}|$ on the relevant positive level region;

(d) The contour-interpolation error;

(e) The unresolved finite-time mask $\mathcal{U}_{N_{\max}}$ defined in (138).

***Remark* 12.2.** Proposition 8.6 certifies the scalar approximation through the pointwise estimate (136). The unresolved step is to convert this scalar certificate, together with grid and interpolation information, into a Hausdorff certificate for an extracted level curve.

12.2. Proposed Geometric Stability Principle

The following conjecture is a proposed intermediate result. A uniform scalar error bound alone does not control the topology of an approximating level set, since additional oscillatory or disconnected components may occur. The conjecture therefore includes a regularity and component-selection hypothesis intended to exclude such spurious components. It should be promoted to a theorem only after a complete proof and a precise formulation of this additional hypothesis have been supplied.

Conjecture 12.3 (Certified Level-Set Displacement Bound). Let $0 < a < b$, and let $\Omega_{a,b}$ be the compact positive-potential band defined in (164). Suppose that $F : \Omega_{a,b} \to \mathbb{R}$ is continuously differentiable and satisfies

$$\left\| F - G_{\mathcal{M}} \right\|_{L^{\infty}(\Omega_{a,b})} \le \varepsilon. \tag{169}$$

Define

$$m_{a,b} := \inf_{c \in \Omega_{a,b}} \left| \nabla G_{\mathcal{M}}(c) \right|. \tag{170}$$

Assume that

$$m_{a,b} > 0. \tag{171}$$

For $t \in [a+\varepsilon, b-\varepsilon]$, define the approximate level set

$$E_t(F) := \left\{ c \in \Omega_{a,b} : F(c) = t \right\}. \tag{172}$$

Assume, in addition, that $E_t(F)$ satisfies a specified regularity and component-selection condition that excludes spurious level-set components and selects the component corresponding to the exact equipotential E_t. Then there should exist a function $\rho_{a,b}(\varepsilon)$, independent of t, such that

$$d_{\mathrm{H}}\left(E_t(F), E_t\right) \le \frac{\varepsilon}{m_{a,b}} + \rho_{a,b}(\varepsilon) \tag{173}$$

for every $t \in [a+\varepsilon, b-\varepsilon]$, where

$$\frac{\rho_{a,b}(\varepsilon)}{\varepsilon} \to 0 \quad (\varepsilon \downarrow 0). \tag{174}$$

Remark **12.4.** The gradient condition (171) is natural in view of the conformal representation (82). Indeed, $G_{\mathcal{M}} = \log|\Phi_{\mathcal{M}}|$, while Theorem 4.8 shows that $\Phi_{\mathcal{M}}$ is conformal and nonvanishing on $\mathbb{C} \setminus \mathcal{M}$. These facts motivate the expectation that the exact potential has no critical points on compact positive-potential bands. A complete proof of the corresponding nonvanishing-gradient statement, together with the existence of a positive lower bound for $|\nabla G_{\mathcal{M}}|$ on $\Omega_{a,b}$, may be included as a preliminary lemma in a future treatment of Conjecture 12.3.

Remark **12.5.** A proof of Conjecture 12.3, together with a precise regularity and component-selection condition, would provide the analytic mechanism needed to convert the pointwise first-escape certificate (136) into a certified geometric error bound of the form (173) for positive equipotentials.

12.3. Target Theorem for Certified Equipotentials

Problem 12.6 (Certified Convergence of Computed Equipotentials). Fix $0 < a < b$. For each $j \ge 1$, let

- $h_j > 0$ be the parameter-grid mesh size;
- N_j be the maximum iteration count;
- R_j be an admissible escape radius;
- $\hat{G}_j$ be the corresponding certified first-escape field;
- $\Gamma_{j,t}$ be the numerical contour extracted at level $t \in [a,b]$.

Assume that $h_j \to 0$, $N_j \to \infty$, and that the certified scalar errors satisfy

$$\sup_{c \in \Omega_{a,b}} \left|\hat{G}_j(c) - G_{\mathcal{M}}(c)\right| \to 0. \tag{175}$$

Under an explicit contour-regularity condition, the computed curves should satisfy

$$\sup_{t \in [a,b]} d_{\mathrm{H}}\left(\Gamma_{j,t}, E_t\right) \to 0. \tag{176}$$

Moreover, the proof should yield a computable estimate of the form

$$d_{\mathrm{H}}\left(\Gamma_{j,t}, E_t\right) \le \mathcal{E}_j(t), \tag{177}$$

where $\mathcal{E}_j(t)$ is calculated from the scalar certificate, the grid resolution, the contour-interpolation error, and a lower bound for $|\nabla G_{\mathcal{M}}|$ on the relevant positive-potential band.

Remark **12.7.** The target result (176) is stronger than numerical convergence observed in a plot. It requires an a posteriori certificate of the form (177) for every computed positive equipotential.

12.4. Adaptive Certified Computation

Problem 12.8 (Certified Adaptive Refinement Criterion). Let Q be a parameter-grid cell. Associate with Q: [label=()]

(i) An upper bound η_Q for the first-escape approximation error on the detected vertices of Q;

(ii) The oscillation $\operatorname{osc}_Q\left(\hat{G}_{\text{esc}}\right)$ of the computed field over Q;

(iii) The mesh diameter h_Q;

(iv) An unresolved-cell indicator $u_Q \in \{0,1\}$.

There should exist an explicit refinement functional

$$\Re(Q) = \Re\left(\eta_Q, \operatorname{osc}_Q\left(\hat{G}_{\text{esc}}\right), h_Q, u_Q\right) \tag{178}$$

with the following properties:

1. If $\Re(Q) \le \varepsilon$, then Q may be accepted without further refinement;
2. If $\Re(Q) > \varepsilon$, then subdividing Q or increasing its iteration budget decreases the certified uncertainty;
3. Repeated refinement terminates on compact positive level ranges.

***Remark* 12.9.** The proposed refinement functional (178) would replace uniform-grid computation by an error-driven method that concentrates numerical effort near the requested equipotential and near cells with unresolved escape behaviour.

12.5. Escape-Time Complexity near the Boundary

Conjecture 12.10 (Escape-Time Growth on Controlled Positive-Potential Layers). Fix an admissible escape radius $R_{\text{esc}} > 2$. For $c \in \mathbb{C} \setminus \mathcal{M}$, define

$$\tau(c) := \min\left\{n \ge 1 : \left|f_c^{\circ n}(0)\right| > R_{\text{esc}}\right\}. \tag{179}$$

Let $\mathcal{P} \subset \mathbb{C} \setminus \mathcal{M}$ be a prescribed class of escaping parameters satisfying a uniform dynamical control hypothesis. Such a hypothesis may, for example, take the form of a uniform non-recurrence condition, a uniform distortion estimate along the critical orbit, or a restriction to a controlled family of external angles. Then there should exist constants $A, B > 0$, depending only on $\mathcal{P}$ and R_{esc}, such that

$$\tau(c) \le A + B \log^{+}\left(\frac{1}{G_{\mathcal{M}}(c)}\right) \quad c \in \mathcal{P}. \tag{180}$$

Equivalently, on a parameter class satisfying the stated uniform dynamical control, the computational effort required for certified first-escape detection should grow at most logarithmically in the inverse Green-function level.

***Remark* 12.11.** The parameter-class hypothesis in Conjecture 12.10 is essential. A global version of (180) may fail because parameters near renormalizable or parabolic regimes can exhibit long transient behaviour. A future treatment should therefore formulate and verify an explicit uniform non-recurrence, distortion, or external-angle condition on $\mathcal{P}$ under which the constants A and B can be computed or bounded.

12.6. Certified External-Ray Approximation

Conjecture 12.12 (Certified Convergence of Compact Numerical Ray Segments). Fix $0 < a < b$ and $\theta \in \mathbb{R}/\mathbb{Z}$. Define the compact positive-potential segment of the parameter external ray by

$$\mathcal{R}_{\theta;[a,b]} := \mathcal{R}_\theta \cap \{c \in \mathbb{C} \setminus \mathcal{M} : a \le G_{\mathcal{M}}(c) \le b\}, \tag{181}$$

where $\mathcal{R}_\theta$ is the exact parameter external ray introduced in Definition 7.1 and (106). Under the parameter Böttcher coordinate, the set $\mathcal{R}_{\theta;[a,b]}$ is the inverse image of the compact radial segment $\{e^t e^{2\pi i\theta} : t \in [a,b]\}$. Since $\Phi_{\mathcal{M}}^{-1}$ is continuous on $\mathbb{C} \setminus \overline{\mathbb{D}}$, the set $\mathcal{R}_{\theta;[a,b]}$ is compact. Moreover, by (165), it is contained in the compact positive-potential band $\Omega_{a,b}$. Suppose that L_K, defined in (150), is evaluated using compatible logarithmic branches on a neighbourhood of $\mathcal{R}_{\theta;[a,b]}$, and let $\mathcal{R}_{\theta;[a,b]}^{(K,h)}$ be the corresponding numerical ray segment extracted from a grid of mesh size h. Then there should exist a computable function $\mathcal{A}(K,h,a,b)$ such that

$$d_{\mathrm{H}}\left(\mathcal{R}_{\theta;[a,b]}^{(K,h)}, \mathcal{R}_{\theta;[a,b]}\right) \le \mathcal{A}(K,h,a,b), \quad \mathcal{A}(K,h,a,b) \to 0 \tag{182}$$

as $K \to \infty$ and $h \downarrow 0$.

***Remark* 12.13.** The restriction $a \le G_{\mathcal{M}} \le b$ places the ray segment in the compact positive-potential band $\Omega_{a,b}$ defined in (164). It therefore separates the problem from ray landing, boundary local connectivity, and the unbounded part of the ray near infinity. The proposed certificate (182) concerns only compact ray segments lying a positive-potential distance from $\partial\mathcal{M}$.

12.7. Scope of the Proposed Programme

The proposed programme focuses on a single unresolved transition: moving from certified scalar approximation of the Green function to certified approximation of exterior geometric objects. In particular, the programme seeks to convert the scalar certificate (136) into geometric estimates such as (177) and (182). The intended outcomes are:

(i) A rigorous conversion of potential error into Hausdorff level-curve error;

(ii) A posteriori certificates for computed positive equipotentials;

(iii) Adaptive refinement criteria with provable termination away from $\partial\mathcal{M}$;

(iv) Quantitative estimates for the cost of first-escape detection;

(v) Branch-certified approximation of compact parameter-ray segments.

The target statements and conjectures in this section are not used in the present paper. They define a proposed research programme building on Theorem 8.1, Proposition 8.6, and Theorem 9.1.

13. Conclusion

This paper places finite critical orbit approximation within the classical conformal and potential-theoretic description of the Mandelbrot exterior. Starting from the normalized Douady–Hubbard parameter Böttcher map of Theorem 4.8, the exterior Green function is constructed through the conformal identity (82). Its harmonicity, positivity, continuous extension by zero, and normalized logarithmic growth are established in Propositions 5.6–5.10 and Theorem 5.8, while Theorem

6.1 characterizes it as the unique normalized exterior Green function of $\mathbb{C}\setminus\mathcal{M}$ with pole at infinity. The central connection is the conformal–dynamical normalization proved in Proposition 5.3, Corollary 5.4, and (81). It identifies the parameter Green function, the parameter Böttcher potential, and twice the critical-point escape rate. Consequently, the finite critical orbit approximants defined in (30) approximate the exact parameter-plane potential. Theorem 8.1 makes this identification quantitative through the explicit exponential error bound (108). Its self-contained telescoping proof explains the decay rate 2^{-n} after the critical orbit enters an admissible escape region. Corollary 8.4 strengthens this pointwise estimate to locally uniform exponential convergence through (124). Thus, every compact subset of $\mathbb{C}\setminus\mathcal{M}$ admits a common entry index and a common error constant, although no analogous global uniform estimate is asserted near $\partial\mathcal{M}$. The numerical methodology distinguishes the fixed-index field (133) from the variable-time first-escape estimator (135). For every parameter whose escape is detected, Proposition 8.6 provides the pointwise certificate (136). By contrast, the unresolved set (138) records only failure to detect escape within the prescribed iteration budget and does not certify membership in $\mathcal{M}$. The convergence visualization compares fixed-index approximants with a certified numerical reference. The reference error is controlled by (156), and the combined comparison estimate is given by (159). The plotted bound (160), implemented by Algorithm 6, therefore remains consistent with the exact analytic normalization. The exact exterior geometry is described by the equipotentials and parameter external rays introduced in Definition 7.1. The conformal pullback identity proved in Proposition 7.2 identifies positive equipotentials with inverse images of Euclidean circles. Using this identity, Theorem 9.1 proves the Hausdorff continuity (161) over compact positive level ranges. The compact positive-potential bands defined in (164) also support the uniform approximation estimate (166). For finite-resolution visualization, the truncated Böttcher logarithm (150) provides numerical potential and external-angle fields through (151) and (152). These fields illustrate the exact conformal geometry but are not used in the analytic proofs. In particular, no global branch-certified error estimate is asserted for the numerical angle field or for the parameter-ray components extracted by Algorithm 4. Taken together, these results clarify the relationship among the dynamical Green function, the parameter Böttcher potential, and finite critical orbit regularization. Classical exterior uniformization supplies the exact analytic object, while the quantitative estimates and certified numerical procedures explain how that object may be approximated from finite orbit data. Viewed alongside [6], the present work provides a conformal and geometric companion to the earlier quantitative study. The limitations in Section 11 and the programme proposed in Section 12 identify the next step: converting certified scalar approximations of $G_{\mathcal{M}}$ into certified geometric approximations of positive equipotentials and compact parameter-ray segments.

Code and Algorithm Availability

The Python programs, numerical experiments, and supporting computational procedures used in this article are available in the author's GitHub notebook:

Exterior_Green_Function_of_the_Mandelbrot_Set.ipynb.

The notebook contains the computational implementations used to generate the numerical and schematic visualizations appearing in the manuscript, namely:

(i) Dynamical-plane and parameter-plane first-escape visualizations, shown in Figure 3;

(ii) Schematic exterior uniformization of the Mandelbrot set, shown in Figure 1;

(iii) Variable-time first-escape visualization of the parameter Green function, shown in Figure 2;

(iv) Numerical exterior geometry of the Mandelbrot set, including Green-function equipotentials and numerical parameter external rays, shown in Figure 4;

(v) Convergence of the normalized escape-rate approximants $2G_n(c)$, shown in Figure 5;

(vi) Nearby positive level curves of the first-escape estimator, shown in Figure 6.

These codes document the implementation of the finite critical orbit approximation, the truncated Böttcher-logarithm approximation, the numerical contour-extraction procedures, and the plotting algorithms described in Section 8.1. The notebook is provided to support reproducibility of the numerical visualizations and to make the computational procedures underlying Figures 3-6 available to readers.

Conflicts of Interest

The author declares no conflicts of interest regarding the publication of this paper.

References

[1] Carleson, L. and Gamelin, T.W. (1993) Complex Dynamics. Springer.

[2] Douady, A. and Hubbard, J.H. (1984) Étude dynamique des polynômes complexes. Partie I. Publications Mathématiques d'Orsay 84-02, Université de Paris-Sud.

[3] Douady, A. and Hubbard, J.H. (1985) Étude dynamique des polynômes complexes. Partie II. Publications Mathématiques d'Orsay 85-04, Université de Paris-Sud.

[4] Hubbard, J.H. (2006) Teichmüller Theory and Applications to Geometry, Topology, and Dynamics, Vol. 1. Matrix Editions.

[5] Milnor, J. (2006) Dynamics in One Complex Variable. 3rd Edition, Princeton University Press.

[6] Moitra, A. (2026) From Asymptotics to Algorithms: Quantitative Regularization of Escape Rates in Quadratic Complex Dynamics. ResearchGate Preprint. https://www.researchgate.net/publication/401923896_From_Asymptotics_to_Algorithms_Quantitative_Regularization_of_Escape_Rates_in_Quadratic_Complex_Dynamics

[7] Brolin, H. (1965) Invariant Sets under Iteration of Rational Functions. *Arkiv för Matematik*, **6**, 103-144. https://doi.org/10.1007/bf02591353

[8] Beardon, A.F. (1991) Iteration of Rational Functions. Springer.

[9] Ransford, T. (1995) Potential Theory in the Complex Plane. Cambridge University Press. https://doi.org/10.1017/cbo9780511623776

[10] Axler, S., Bourdon, P. and Ramey, W. (2001) Harmonic Function Theory. 2nd Edition, Springer.

[11] DeMarco, L. (2003) Dynamics of Rational Maps: Lyapunov Exponents, Bifurcations, and Capacity. *Mathematische Annalen*, **326**, 43-73. https://doi.org/10.1007/s00208-002-0404-7

[12] Dujardin, R. and Favre, C. (2008) Distribution of Rational Maps with a Preperiodic Critical Point. *American Journal of Mathematics*, **130**, 979-1032. https://doi.org/10.1353/ajm.0.0009

[13] Favre, C. and Gauthier, T. (2018) Continuity of the Green Function in Meromorphic Families of Polynomials. *Algebra & Number Theory*, **12**, 1471-1487. https://doi.org/10.2140/ant.2018.12.1471

[14] Dudko, D. and Lyubich, M. (2023) Local Connectivity of the Mandelbrot Set at Some Satellite Parameters of Bounded Type. *Geometric and Functional Analysis*, **33**, 912-1047. https://doi.org/10.1007/s00039-023-00637-8

[15] Dudko, D., Lyubich, M. and Selinger, N. (2020) Pacman Renormalization and Self-Similarity of the Mandelbrot Set near Siegel Parameters. *Journal of the American Mathematical Society*, **33**, 653-733. https://doi.org/10.1090/jams/942

[16] Buff, X. and Chéritat, A. (2012) Quadratic Julia Sets with Positive Area. *Annals of Mathematics*, **176**, 673-746. https://doi.org/10.4007/annals.2012.176.2.1

[17] Wang, X. (2026) Continuity of Julia Sets and Invariant Rays. arXiv: 2602.20588.

[18] Zhang, R. (2025) Parabolic Implosion in the Parameter Space of Cubic Polynomials. arXiv: 2508.16430.

[19] Hare, K.G. and Noytaptim, C. (2024) Totally Real Algebraic Numbers in Generalized Mandelbrot Set. arXiv: 2405.10395.

[20] Astorg, M., Benini, A.M. and Fagella, N. (2026) A Universal Model for the Bifurcations of Asymptotic Values. arXiv: 2603.15466.

[21] Harris, C.R., Millman, K.J., van der Walt, S.J., Gommers, R., Virtanen, P., Cournapeau, D., *et al.* (2020) Array Programming with NumPy. *Nature*, **585**, 357-362. https://doi.org/10.1038/s41586-020-2649-2

[22] Hunter, J.D. (2007) Matplotlib: A 2D Graphics Environment. *Computing in Science & Engineering*, **9**, 90-95. https://doi.org/10.1109/mcse.2007.55